# A tonoplast-localized magnesium transporter is involved in stomatal opening in Arabidopsis

**Shin-ichiro Inoue** ( shin@bio.nagoya-u.ac.jp )
Nagoya University
**Maki Hayashi**
Nagoya University
**Sheng Huang**
Okayama University https://orcid.org/0000-0002-2868-4331
**Kengo Yokosho**
Okayama University
**Eiji Gotoh**
Kyushu University
**Shuka Ikematsu**
Institute of Transformative Bio-Molecules (ITbM), Nagoya University
**Masaki Okumura**
Nagoya University
**Takamasa Suzuki**
Chubu University https://orcid.org/0000-0002-1977-0510
**Takumi Kamura**
Nagoya Univdersity
**Toshinori Kinoshita**
Nagoya University https://orcid.org/0000-0001-7621-1259
**Jian Feng Ma**
Okayama University https://orcid.org/0000-0003-3411-827X

**Article**

**Keywords:** Plant stomata, stomatal opening, Arabidopsis

**Posted Date:** December 1st, 2021

**DOI:** https://doi.org/10.21203/rs.3.rs-1023290/v1

**Article**

# A tonoplast-localized magnesium transporter is involved in stomatal opening in Arabidopsis

Shin-ichiro Inoue[1]*, Maki Hayashi[1], Sheng Huang[2], Kengo Yokosho[2], Eiji Gotoh[3], Shuka Ikematsu[4], Masaki Okumura[1], Takamasa Suzuki[5], Takumi Kamura[1], Toshinori Kinoshita[1,4]*, Jian Feng Ma[2]*

[1] Division of Biological Science, Graduate School of Science, Nagoya University, Furo-cho, Chikusa-ku, Nagoya, Aichi 464-8602, Japan
[2] Institute of Plant Science and Resources, Okayama University, Chuo 2-20-1, Kurashiki, 710- 0046, Japan
[3] Department of Biology, Faculty of Science, Kyushu University, 744 Motooka, Fukuoka 819-0395, Japan
[4] Institute of Transformative Bio-Molecules (WPI-ITbM), Nagoya University, Chikusa, Nagoya 464-8602, Japan
[5] Department of Biological Chemistry, College of Bioscience and Biotechnology, Chubu University, Kasugai-shi, Aichi, Japan

*Corresponding authors

Corresponding authors:
**Shin-ichiro Inoue**
Division of Biological Science, Graduate School of Science, Nagoya University, Furo-cho, Chikusa-ku, Nagoya, Aichi 464-8602, Japan
Tel/Fax: +81-52-789-4780
E-mail: shin@bio.nagoya-u.ac.jp
**Toshinori Kinoshita**
Institute of Transformative Bio-Molecules (WPI-ITbM), Nagoya University, Chikusa, Nagoya 464-8602, Japan
Tel/Fax: +81-52-789-4780
E-mail: kinoshita@bio.nagoya-u.ac.jp
**Jian Feng Ma**
Institute of Plant Science and Resources, Okayama University, Chuo 2-20-1, Kurashiki, 710- 0046, Japan

Tel/Fax: 81-86-434-1209
E-mail: maj@rib.okayama-u.ac.jp

**Abstract**

Plant stomata play an important role in $CO_2$ uptake for photosynthesis and transpiration, but the mechanisms underlying stomatal opening and closing are still not completely understood. Here, through large-scale screening, we identified an Arabidopsis mutant (*cst2 for closed stomata2*) defective in stomatal opening under light condition. A map-based cloning combined with complementation test revealed that the mutant phenotype was caused by a nucleotide substitution of a gene, which domains show similarity to human Mg efflux transporter ACDP/CNNM. Functional analysis showed that *CST2* encodes a tonoplast-localized transporter for Mg. This protein is constitutively and highly expressed in the guard cells. Furthermore, CST2 is phosphorylated by calcineurin B-like protein (CBL)-interacting protein kinases 26 (CIPK26) *in vitro*, which is probably required for its activation. Knockout of this gene resulted in stomatal closing and growth retardation under high Mg concentration conditions, while over-expression of this gene increased tolerance to high Mg. Our results indicate that CST2 plays an important role in maintaining Mg homeostasis in plant cells through sequestering Mg into vacuoles especially in guard cells and that this homeostasis is required for stomatal opening, which provide a novel insight into mechanism of stomatal opening in plants.

**Introduction**

Stomatal pores, formed by pairs of guard cells in the plant epidermis, regulate gas exchange between plants and the atmosphere. Stomatal opening is required for $CO_2$ uptake for photosynthesis and water transpiration for maintaining leaf temperature [1, 2]. A number of studies have done on the mechanisms of stomatal opening and closing in different plant species especially in model plant Arabidopsis. Among them, light has been demonstrated to be a key environmental cue to induce stomatal opening under natural conditions. The stomatal responses to light are regulated by two distinct light-activated signaling pathways: a blue light pathway and a photosynthetically active radiation (PAR)-dependent pathway [2-4]. Blue light acts directly on guard cells to induce stomatal signaling, while PAR acts directly and indirectly on guard cells. It has been suggested that guard cell photosynthesis generates ATP or other metabolic processes for stomatal opening [5-7] and mesophyll cell photosynthesis induces a

decrease of $CO_2$ in the leaves, which acts on guard cells to mediate the opening of stomata [2, 6, 8].

Stomatal opening is driven by the guard cell-swelling in response to blue light, suggesting that a single guard cell possesses all signaling components, from blue light-perception to cell-volume increase, for stomatal opening [2, 9]. Blue light activates the plasma membrane $H^+$-ATPase via photoreceptor phototropin-mediated signaling [10, 11]. The activated $H^+$-ATPase hyperpolarizes the plasma membrane, followed by activation of inward-rectifying $K^+$ channels [12-14]. In addition, phototropin signaling distinct from the $H^+$-ATPase pathway activates the $K^+$ channels via CBL-interacting protein kinase 23 (CIPK 23) [15, 16]. Theses $K^+$ channel activation induces an influx of $K^+$, resulting in the accumulation of $K^+$ and the counter anions of $Cl^–$, nitrate ($NO_3^-$) and malate$^{2–}$ in a guard cell. $K^+$ and $Cl^–$ are transported into the vacuole via the tonoplast-localized transporters NHX1 and NHX2, and channels ALMT9 and CLCc, respectively [17-20]. Accumulation of these ions decreases the guard cell-water potential, leading to water uptake into the vacuole and turgor increase, which finally induces stomatal opening [14, 21]. Apart from these ion transport events, starch degradation in guard cell chloroplasts is induced downstream of phototropin-activated $H^+$-ATPase, which also contributes to stomatal opening without affecting the capacity of guard cell-ion transports [22, 23]. However, these signaling and the regulatory mechanisms for each event are not completely elucidated and our understanding of stomatal opening is still not sufficient.

In this study, to identify novel factors involved in stomatal opening, we performed a large-scale screening of mutants defective in stomatal opening in Arabidopsis using infrared thermography. Through gene mapping and detailed functional analysis of one mutant (*cst2* for *closed stomata 2*), we found that a tonoplast-localized transporter for Mg, CST2 is involved in stomatal opening in Arabidopsis.

## Results

### Isolation and physiological characterization of a mutant defective in stomatal opening

To further understand the mechanisms involved in stomatal opening, we performed a large-scale genetic screening of Arabidopsis mutants using infrared thermography [24]. We obtained several mutants (designated *closed stomata* (*cst*)) showing higher leaf temperature than WT, due to the impairment of stomatal opening. We have functionally characterized the first mutant *cst1* [24], and in this study we report the second mutant *cst2-1*, which also showed higher leaf temperature and retarded growth (Fig. 1a). Physiological analysis showed that *cst2-1* exhibited smaller stomatal opening than the wild type (WT) under both light and dark conditions (Fig. 1b), but the difference in stomatal opening between *cst2-1* and WT was larger under light condition. *cst2-1* mutant showed reduced photosynthetic electron transfer to PSII compared to WT (Fig. 1c). The growth of *cst2-1* was greatly decreased compared with the WT (Fig. 1d). Intriguingly, when grown under drought stress condition, the WT was wilted, but the mutant survived well (Fig. 1e), probably due to stomata closure to prevent water loss. All these observations indicate that the phenotype of *cst2-1* is caused by defect of stomatal opening under light condition.

### Gene mapping and complementation test

In order to map the gene responsible for the *cst2-1* phenotype, we performed map-based cloning and sequence analysis using the next-generation sequencer. As a result, we identified a single nucleotide substitution from guanine (G) to adenine (A) at the sixth intron splicing acceptor site of the AT4G14240 gene (Supplementary Fig. 1a). Western blot analysis indicated that there was no CST2 protein detected (Supplementary Fig. 1b). To confirm this mapping result, we performed a complementation test by introducing the wild-type *CST2* gene into *cst2-1* mutant. Analysis with three independent lines showed that *CST2* completely restored growth defect and stomatal opening of *cst2-1* mutant (Supplementary Fig. 1c, d). Furthermore, we obtained a T-DNA insertion line (GABI_322H07), which is designated as *cst2-2* (Supplementary Fig. 1a). There was no expression of *CST2* gene and protein in this line (Supplementary Fig. 1b, e). Furthermore, *cst2-2* showed similar phenotypes to *cst2-1* in terms of growth, stomatal opening and photosynthesis (Fig. 1b, c, d), indicating that *cst2-2* is also a knockout mutant of *CST2*.

**Phylogenetic analysis of CST2**

CST2 encodes an uncharacterized protein with a Domain of Unknown Function 21 (DUF21) and a cytosolic cystathionine-b-synthase (CBS)-pair domain (Supplementary Fig. 2a). In *Arabidopsis* genome, there are six homologs of CST2 with similarity ranging from 43.6 to 82.4% (Supplementary Fig. 2b). Blast search revealed that the domains of CST2 protein are found in archaea, bacteria, fungi, algae, plants, and animals (Supplementary Fig. 2c). Among them, bacterial homologs, CorB and MpfA were reported to mediate Mg efflux [25-27], and archaeal CorB showed Mg transport activity *in vitro* [28]. Animal homolog ACDPs/CNNMs were also implicated in Mg transports although it was unclear whether CNNM proteins are Mg transporters or regulators of other Mg transporters [29, 30]. MAM3, a homolog of CST2 in yeast (Supplementary Fig. 2c) was reported to be associated with manganese (Mn) homeostasis and located to the tonoplast, but its exact role in Mg homeostasis is unknown [31].

**Transport activity and subcellular localization of CST2**

To test whether CST2 was also able to transport Mg like its homologs in other organisms, we performed yeast assay using a yeast mutant, *mam3*. When yeast was grown in SOD medium containing 3 mM Mg, *mam3* knockout mutant showed reduced Mg accumulation compared to WT (Fig. 2a: Empty/ WT vs Empty/ *mam3*). This mutant phenotype was completely recovered by both introduction of WT *MAM3* gene and *Arabidopsis CST2* gene (Fig. 2a: Empty/ *mam3* vs MAM3/ *mam3* and CST2/ *mam3*). These results indicate that CST2 functions as an ortholog of MAM3 and that both MAM3 and CST2 are able to transport Mg.

We then investigated the subcellular localization of CST2 by transiently expressing CST2-GFP fusion with tonoplast marker (Tonoplast target signal (TTS)-mCherry) and plasma membrane marker (mCherry-AHA1) in *Nicotiana benthamiana* leaves (Fig. 2b). The result showed that the fluorescence signal from CST2-GFP was well merged with tonoplast marker. These results indicate that similar to MAM3, CST2 protein is also localized to the tonoplast.

**Expression pattern of *CST2***

We examined the expression pattern of *CST2* by qRT-PCR. The expression of *CST2* was higher in the leaves than in the roots (Fig. 2c). The expression in both the roots and shoots did not respond to Mg-deficiency and –excess (Fig. 2c).

Western blot analysis showed that CST2 protein accumulation was not altered by high Mg (20 mM) up to 72 hours (Fig. 2c). Furthermore, accumulation of the CST2 protein was not changed in response to 5, 10, 20 mM Mg supply compared with 0 mM Mg (Fig. 2d). These results indicate that CST2 is constitutively expressed at both transcriptional and protein levels.

We further investigated expression patterns of *CST2* using transgenic plants expressing the *GUS* reporter gene under the control of native *CST2* promoter. Consistent with qRT-PCR result (Fig. 2c), GUS signal was ubiquitously observed in both the roots and leaves with stronger signal in the leaves (Fig. 3a-c, f, g). In the leave, a strong signal was observed in the guard cells (Fig. 3d, e) and vascular bundle tissues (Fig. 3c, d, f, h, i). Expression of CST2 protein was also confirmed by western blot analysis in guard cells, mesophyll cells, leaves, and roots (Fig. 3j).

**Effect of different Mg concentrations on growth of *cst2* mutants and over-expression lines**

To investigate the role of CST2 in Mg homeostasis, we compared the growth between WT and two independent *cst2* mutants at different Mg concentrations including 0.25, 1, and 5 mM. When WT and *cst2* mutants were grown hydroponically for 4 weeks at 0.25 mM Mg, the growth of both the roots and shoots were almost similar (Fig. 4a-c). However, at 1 (a concentration for normal growth) and 5 mM Mg, the growth of both the roots and shoots of *cst2* mutants were significantly decreased compared with the WT (Fig. 4a-c). We further tested whether this response is specific to high Mg by exposing the plants to different ions. The results showed that the growth difference between WT and *cst2* mutants was only observed at high Mg concentration (Supplementary Fig. 3). These results indicate that knockout of *CST2* specifically increased sensitivity to high Mg concentrations.

We also generated over-expression lines of *CST2*. The over-expression lines showed higher accumulation of CST2 proteins (Supplementary Fig. 4a). Over-expression of *CST2* significantly enhanced tolerance to high Mg concentrations compared with the WT (Supplementary Fig. 4b). At Mg concentrations above 35 mM, the overexpression lines were able to survive, whereas WT died.

We compared Mg concentration in the leaves between WT and *cst2* mutants. The results showed that at low Mg concentration (0.75 mM), the leaf Mg concentration was similar between WT and *cst2* mutant (Fig. 4d). However, at

high Mg concentration (5.75 mM), the mutants contained lower Mg concentration than the WT. This decrease in Mg accumulation could be attributed to disrupted Mg homeostasis in the cells. Higher Mg concentration in cytosol in the mutant may down-regulate transporter genes involved in Mg uptake although further investigation is required.

**Mg homeostasis is associated with stomatal opening.**

To link Mg homeostasis with stomatal opening, we investigated the light-dependent stomatal opening of *cst2* mutants and WT at various Mg concentrations. Stomata in the WT leaves opened to a similar extent in response to Mg from 0.05 to 5 mM under light condition. However, stomata in the *cst2-1* leaves opened only at Mg concentrations from 0.05 to 0.2 mM under light condition (Fig. 5a). The stomata opening in *cst2* mutants was completely suppressed at a Mg concentration of 0.75 mM or higher.

We further investigated Mg-dependent stomatal opening in a time-dependent manner. The stomatal opening capacities of the mutants started to decrease at 24 hours after the plants were transferred from 0.2 to 5 mM Mg (Fig. 5b). By contrast, the stomatal opening capacity of WT was hardly changed over time under the same conditions. We also compared stomatal conductance and photosynthetic rate between the WT and *cst2* mutants. Magnitude and rate of stomatal conductance were reduced in *cst2* mutants compared to those in WT (Fig. 5c). Photosynthetic rate of *cst2* mutant leaves was also reduced (Fig. 5d). These results suggest that Mg homeostasis is important for stomatal opening and photosynthesis.

**Functional relationship between CST2 and CBL-CIPK complex**

It was reported that the tonoplast-localized calcium sensors, the calcineurin B-like (CBL) 2 and CBL3 and their regulating partners, CBL-interacting protein kinase (CIPK) 3, CIPK9, CIPK23, and CIPK26 are involved in regulation of Mg homeostasis through Mg sequestration into vacuoles [32, 33]. However, it is unknown whether CST2 is regulated by the CBL-CIPK complexes. Because the *cbl2 cbl3* double mutant also showed similar phenotype to *cst2* mutants (Mg hypersensitive and low Mg accumulation) [32], we therefore, examined the possible interaction between CST2 and CBL2/3. We first compared Mg sensitivity among *cst2-1*, *cbl2 cbl3*, and *cst2-1 cbl2 cbl3* mutants (Fig. 6a). The *cbl2 cbl3* mutant showed a weaker growth inhibition than the *cst2-1* mutant in response to high Mg

supply. The Mg-hypersensitive phenotype of *cst2-1 cbl2 cbl3* triple mutant was similar to that of *cst2-1* (Fig. 6b). These results indicate that CST2 and CBL2/3 work on the same signaling pathway. We further investigated the effect of *CST2* overexpression on Mg sensitivity in the *cbl2 cbl3* background. Overexpression of CST2-GFP largely recovered the hypersensitive phenotype of the *cbl2 cbl3* mutant (Fig. 6b), indicating that CST2 functions downstream of CBL2/3 in the same signaling pathway.

We then examined the protein-protein interaction between CST2 and CIPK26 using an *in vitro* pull-down assay. Recombinant GST-CIPK26 and GST-SRK2E were used as baits and incubated with recombinant His-CST2 C-terminal fragment (CST2 C-ter). CIPK26 interacted with CST2 but SRK2E as a control did not *in vitro* (Fig. 6c). Bimolecular fluorescence complementation (BiFC) assay in *Nicotiana benthamiana* leaves further confirmed the interaction between CIPK26 and CST2 (Fig. 6d).

We finally performed *in vitro* phosphorylation assay using the recombinant GST-CIPK26 and His-CST2 C-ter. The result showed that CIPK26 effectively phosphorylated CST2 *in vitro* (Fig. 6e: WT). This phosphorylation was completely abolished by a mutation that lost CIPK26 catalytic activity (Fig. 6e: K.D.).

**Discussion**

Stomatal opening in plant leaves is caused by the swelling of a pair of guard cells, which is achieved by increasing cell volume through ion accumulations followed by water influx [2, 34]. Until now, it has been reported that accumulation of ions including $K^+$, $Cl^-$, and nitrate ($NO_3^-$), and malate$^{2-}$ in guard cells, in particular, the accumulation of $K^+$ and $Cl^-$ in the vacuoles largely contributes to the cell volume increase of guard cells [20, 34]. In this study, we identified a novel component required for stomatal opening, CST2. CST2 is a tonoplast-localized transporter for Mg with high expression in the guard cells (Figs. 2a, 2b, 3). Knockout of this gene resulted in stomatal closure under high Mg concentrations (Fig. 5a-c), whereas its over-expression enhanced the tolerance to high Mg (Supplementary Fig. 4b). Our results revealed that sequestration of Mg by CST2 into the vacuole is required for stomatal opening under high Mg concentration conditions. There are at least three possibilities for involvement of CST2 in stomatal opening. The first one is that CST2 mediates transport of Mg into the vacuoles of guard cells (Fig. 7), which contributes to increase in the osmotic pressure for guard cell-swelling. However, this possibility is unlikely because *cst2* mutants also showed

similar stomatal opening as WT at low Mg concentrations (Fig. 5a). The second possibility is that Mg homeostasis in the guard cells affects other components involved in stomatal opening (Fig. 7). Although Mg is an essential element for plant growth and development, excess Mg in the cytosol due to lack of vacuolar sequestration may cause toxicity, which affects other events involved in stomatal opening. In fact, it was reported that excess Mg inhibits photosynthetic activity through affecting the stroma pH [35, 36]. Because the guard cell photosynthesis provides ATP and/or reducing equivalents, which are the fuel for stomatal opening [5-7], inhibition of guard cell photosynthesis by high Mg may result in stomatal closure. The third possibility is that disruption of the Mg homeostasis in cells other than guard cells induces suppression of stomatal opening. Previous studies of stomatal opening have focused on the signaling within a guard cell, but the effects of other cells on guard cells were not considered except for a phytohormone ABA and $CO_2$ [2, 8, 37]. Nerveless further investigation is required for examining these possibilities in future.

So far, several Mg transporters have been identified in plants [38, 39]. Among them, Mg transporter (MGT/MRS2) family, which is the homologs of the bacterial CorA has been reported to be involved in Mg uptake, internal translocation and vacuolar sequestration [40-44]. For example, MGT2 and MGT3 were reported to be involved in the Mg sequestration into vacuoles [45]. A $Mg^{2+}/H^{+}$ antiporter, MHX was also implicated in vacuolar sequestration of Mg [46]. However, unlike *cst2*, both *mgt2 mgt3* and *mhx* mutants did not exhibit growth retardation in response to high Mg conditions [32], indicating the presence of other vacuolar transporters for sequestering Mg into vacuoles [32, 47]. Our findings in this study indicate that CST2 is the missing transporter for vacuolar sequestration of Mg in plants. This is supported by subcellular localization, transport activity and phenotypic analysis of *cst2* mutants (Figs. 2, 4). Furthermore, CST2 represents a novel type of Mg transporters identified in plants (Supplementary Fig. 2). Since its homologs such as MpfA, CorB, and CNNMs are present in archaea, bacteria, and animals and have been associated with Mg export from a cell [25-27, 48], indicating that Mg transport by CST2-type transporters is evolutionally conserved in different organisms. However, they show different subcellular localization. For example, MpfA, CorB, and CNNMs are localized to the plasma membrane, while plant CST2 is localized to the tonoplast (Fig. 2b). These differences in subcellular localization suggest that they play different roles in Mg utilization in different organisms. Different from animals, plants have developed vacuoles that occupy

about 90% of the cell volume, therefore sequestration of Mg into the vacuoles by CST2 is an importance step for maintaining Mg homeostasis in the cytosol in plants.

Recently, it was demonstrated that the tonoplast-localized calcium sensors, the calcineurin B-like proteins (CBLs) and their regulating partners, CBL-interacting protein kinases (CIPKs) regulates Mg homeostasis through Mg sequestration into vacuoles [32, 33, 38]. Our results revealed that CST2 is one of the target transporters phosphorylated by CBLs-CIPKs (Fig. 6e). This is supported by the genetic, physiological, and physical evidence presented in this study（Fig. 6-d）. Phosphorylation of CST2 is probably required for activating its transport activity although further investigation is required.

In summary, CST2 is a novel type transporter of Mg, which is involved in stomatal opening in Arabidopsis. Its localization at the tonoplast functions to sequester Mg into the vacuoles, which is important for maintaining Mg homeostasis in guard cells and subsequently for stomatal opening. Our work provides novel insights into regulation of stomatal opening in plants.

## Methods

### Screening of mutants defective in stomatal opening

Ethyl methanesulfonate-mutagenized M2 seeds purchased from Lehle Seeds (the trichome-less *glabra1* background), were used for screening of mutants as described previously (Inoue et al., 2017). Plants were grown in soil under a 14 h white light (50 mmol $m^{-2}$ $s^{-1}$) and 10 h dark cycle at 20–25°C at a relative humidity of 55–75% in a temperature-controlled growth room. At 21-25 days, leaf temperature was measured using an infrared thermograph (TVS-500EX; NEC Avio Infrared Technology). Plants were grown for 3 weeks and thermal images were taken at 3-4 h after the start of the light period. Thermal images were analyzed using the Avio Thermography Studio software (NEC Avio Infrared Technology) (Fig. 1a). A mutant showing high leaf temperature, designated as *cst2-1* for *closed stomata 2* was used in this study.

### Plant materials and growth conditions

*Arabidopsis thaliana* Col-0 was used as a wild type (WT). T-DNA insertion mutants (Col-0 background), *cst2-2* (GABI_322H07), *cbl2* (SALK_151426), and *cbl3* (SAIL_785C10) were obtained from the Arabidopsis Biological Resource Center (ABRC) and Nottingham Arabidopsis Stock Centre (NASC). All lines

including *cst2-1* were grown on soil or nutrient solution with a 14 h light/10 h dark photoperiod under white fluorescent light (50 μmol $m^{-2}$ $s^{-1}$) at 22–24°C.

Hydroponic cultivation was performed using the Araponics Growing System (Araponics; http://www.araponics.com/). Plants were grown on 1/2 MS agar medium for 7 days, and then transferred to a nutrient solution [49]. The solution was constantly aerated and replaced every 4 days.

For agar medium growth, plants were grown on 1/2 Murashige and Skoog (MS) agar medium (0.8% (w/v) agar, 0.05% (w/v) MES, pH5.8) with or without $MgSO_4$ supplement at various concentrations.

**Physiological characterization of *cst2* mutants**

To characterize the phenotypes of *cst2* mutants, leaf temperature, stomatal aperture, photosynthetic electron transfer, shoot fresh weight, drought tolerance, and Mg concentration were measured and compared with WT as described below.

For growth comparison, plants were grown on soil. After 4 weeks, the aerial parts were harvested and the fresh weight was recorded. To compare the growth at various Mg concentrations, seeds were sown on 1/2 MS agar medium. After 7-d growth, the seedlings were transplanted to a nutrient solution containing different Mg concentrations. After 4 weeks, the shoots and roots were harvested and dried at 70°C for at least 3 days. To compare the sensitivity to different ionic stress, plants of both WT and *cst2* mutant were grown in 1/2 MS agar medium for 7 days, followed by transferring to a new 1/2 MS media containing different ions at high concentration as shown in Supplementary Fig. 3. Plants were further grown in the new media for 2 weeks and then photographed

For measurement of photosynthetic electron transfer, plants were grown in soil under light at 200 μmol $m^{-2}$ $s^{-1}$ for 5 weeks and then subjected to the measurement as described below. To evaluate drought-tolerance, plants of both WT and *cst2* mutant were first grown on soil for 24 days with watering, followed by stopping watering. After a further 16-d growth under drought stress condition, the plants were photographed. For comparison of Mg concentration, seedlings of WT and *cst2* mutant were grown on 1/2 MS agar medium with or without 5 mM $MgSO_4$ for 3 weeks. The shoots were harvested and washed with Milli Q water 4 times and dried at 70°C for at least 3 days. The dried samples were digested with concentrated $HNO_3$ (60%) at 140 °C. The concentration of Mg in digest solution was determined using ICP-MS (7700X; Agilent Technologies) as described previously [50].

**Measurement of stomatal aperture and stomatal conductance**

For stomatal aperture measurements, the seedlings (4-week-old) grown in soil or hydroponically were kept in the dark before measurement. Rosette leaves were harvested from the dark-adapted plants, and epidermal fragments were isolated using a Waring blender (Waring Commercial) under dim red light. The epidermal fragments were collected on a 58 μm nylon mesh and used for stomatal aperture measurement according to Inoue et al. (2008b) [11] and de Carbonnel et al. (2010) [51] with some modifications. Briefly, to determine the stomatal opening, the epidermal fragments were incubated in 2 ml buffer (5 mM MES/bistrispropane (pH 6.5), 50 mM KCl, and 0.1 mM $CaCl_2$), and illuminated with light for 3 h at room temperature. Stomatal apertures were measured using a microscopy in the abaxial epidermis by focusing on the inner lips of stomata. To investigate the effect of different Mg concentrations on stomatal opening, plants were grown for 4 weeks in a hydroponic solution [49] containing various Mg concentrations before subjecting to stomatal aperture measurement.

To investigate the time course of stomatal opening capacities in response to high Mg, plants were grown in a hydroponic solution containing 0.2 mM Mg for 4 weeks, and then transferred to a solution containing 5 mM Mg and grown for further 5 days. Rosette leaves were harvested 3 h after the start of the light period. Epidermal fragments were immediately isolated and stomatal apertures were determined as described above. Stomatal conductance in intact leaves of WT and *cst2* mutants was determined according to Doi et al. (2004) [52] and Gotoh et al. (2019) [53]. Plants 5days after the transfer to the 5 mM Mg condition were used to measure.

**Chlorophyll fluorescence-based photosynthesis analysis**

For measurement of quantum yield of electron transfer to PSII (ΦPSII), chlorophyll fluorescence yield was measured with a FluorCAM (Photon System Instruments) in plants grown at 200 μmol $m^{-2}$ $s^{-1}$. Minimum fluorescence ($F_o$) was determined by a weak light after dark treatment for 30 min. Steady-state fluorescence (Fs) in illuminated leaf was measured in actinic light at 200 μmol $m^{-2}$ $s^{-1}$. Maximum fluorescence ($F_m'$) in light was determined by a saturating light pulse under actinic light at 200 μmol $m^{-2}$ $s^{-1}$. Quantum yield of electron transfer to PSII (ΦPSII) was calculated as (Fm'-Fs)/Fm.

**Mapping of responsible gene**

To map the gene responsible for *cst2* phenotype, homozygous *cst2-1* mutant in the Col accession background were crossed with Ler accession to generate mapping population. Based on growth retardation of $F_2$ seedlings grown in soil and polymorphism markers distributed throughout the five Arabidopsis chromosomes, the responsible gene was located on chromosome 4. To further identify the responsible mutation, genomic DNA was extracted from the bulked seedlings showing mutant and WT phenotypes and used for library construction for sequencing. A total of 1.99 G bp, approximately 17-fold the size of the Arabidopsis genome, was sequenced, and the obtained short reads were analyzed and compared by the Mitsucal computer system [54] for identification of *cst2* mutation.

**Transport assay of Mg in yeast**

To determine transport activity of CST2 for Mg, yeast mutant *mam3* was used. Yeast strain BY4741 as WT and *mam3* mutant (4741, *mam3 Δ:: KAN*$_R$) were purchased (Thermo). *MAM3* coding sequence and *CST2* cDNA were amplified from yeast genome, and Arabidopsis cDNA, respectively using the primers 5'-TAGAACTAGTGGATCCATGTCGTTTTTGCCACTAAGGTCTAG-3' and 5'-TGACTCGAGGTCGACTCATCTTTTTATGGTCGACGAGGAG-3' for *MAM3* and 5'-CGGGATCCATGCATCTGATTAATGCGGTGGC-3' and 5'-CGGGATCCTCAGTTGTTTCTTCGAATCGGCTCGG-3' for *CST2*. The DNA fragments of *MAM3* and *CST2* were cloned into pRS415-ADH vector [55] using the In-Fusion cloning system (Clontech). The resulting and empty vectors were introduced into yeast WT and/or *mam3* mutant and used for measurement of Mg concentration.

Yeast cells were grown in SD medium containing 3 mM Mg for 14 h and then harvested by centrifugation. After 4 times washes with Milli Q water, cell pellets were dried at 70°C for at least 3 days. The concentration of Mg in the dried cells were measured as described above.

**Expression analysis of *CST2* by qRT-PCR**

To examine the expression pattern of *CST2*, seedlings (7-week-old) of WT prepared as above were transferred to a nutrient solution containing 0, 0.4 and 5 mM Mg. After 2 days, roots and leaves were sampled for RNA extraction with four biological replicates. Total RNA was extracted using an RNeasy Plant Mini Kit

(Qiagen), and then converted to cDNA by ReverTra Ace qPCR RT Master Mix with gDNA Remover (Toyobo). The expression of *CST2* was determined by quantitative real time PCR (qRT-PCR) with KOD SYBR qPCR Mix (TOYOBO) on a real-time PCR machine (model no. CFX96; Bio-Rad) using the primers: 5'-CATACTTCAGAGGCTATCGAGG-3' (forward) and 5'-TGCTGCTACTCGAATCCTTTTA-3' (reverse). *Actin* was used as an internal standard using primers: 5'-GAGACTTTCAATGCCCCTGC-3' (forward) and 5'-CCATCTCCAGAGTCGAGCACA-3' (reverse). The relative expression was normalized based on *Actin* by the ΔΔCt method.

To confirm expression of *CST2* mRNA in *cst2-2*, total RNA was isolated from rosette leaves of 3-week-old WT and *cst2-2* plants using NucleoSpin RNA Plant (TaKaRa). First-strand cDNA was synthesized from the RNAs using the PrimeScript II 1st Strand cDNA Synthesis Kit (TaKaRa). The *CST2* and *TUB2* fragments were amplified from cDNAs by PCR using the specific primers 5'-ACAAACACAGAGAGATTCATCATCG-3' and 5'-ATGGATCAAAGTATACAGAAGAACC-3' for *CST2* and 5'-CATTGTTGATCTCTAAGATCCGTG-3' and 5'-TACTGCTGAGAACCTCTTGAG-3' for *TUB2*. The *TUB2* fragment was used as an internal standard.

**Subcellular localization of CST2**

CST2-GFP, TTS-mCherry, and mCherry-AHA1 were transiently expressed in leaves of *Nicotiana benthamiana* grown in soil as described above under the control of 35S promoter. The full-length cDNA of each gene was amplified by PCR using primers: 5′-CATGCCATGGCAATGCATCTGATTAATGCGGTGGC-3′ and 5′-CATGCCATGGCGTTGTTTCTTCGAATCGGCTCGG-3′ for *CST2*, 5′-CATGCCATGGCAATGTCGCAGTGCGTTGACGGTATC-3′ and 5′-CATGCCATGGCAAATAAAACACCCTAAAACAGAGG-3′ for *TTS*, and 5′-CCGGTGTACAAGATGTCAGGTCTCGAAGATATCAAG-3′ and 5′-CCGGTGTACAAGCACAGTGTAGTGATGTCCTG-3′ for *AHA1*. The fragments amplified were cloned into the *Nco*I or *Bsr*GI site of the CaMV35S-sGFP(S65T)-NOS3′ vector or the CaMV35S-mCherry-NOS3′ vector. The cDNA of the *CST2-GFP, TTS-mCherry*, and *mCherry-AHA1* were amplified by PCR from the resulting vector using primers 5′-CATATGCCCGTCGACATGCATCTGATTAATGCGGTGGC-3′ and 5′-TCAGAATTCGGATCCTTACTTGTACAGCTCGTCCATGCC-3′ for *CST2-GFP*,

5′-CATATGCCCGTCGACATGTCGCAGTGCGTTGACGGTATC-3′ and 5′-TCAGAATTCGGATCCTTACTTGTACAGCTCGTCCATGC-3′ for *TTS-mCherry*, and 5′-CATATGCCCGTCGACATGGTGAGCAAGGGCGAG-3′ and 5′-TCAGAATTCGGATCCCTACACAGTGTAGTGATGTCCTG-3′ for *mCherry-AHA1*. They were cloned into the downstream of 35S promoter of pRI101-AN DNA vector (Takara) using the In-Fusion cloning system. The resulting construct was introduced into *N. benthamiana* leaves using an *Agrobacterium*-mediated transformation method [16, 56]. Agrobacterium GV3101 strain was transformed with the vector and cultured at 28 °C for about 20 h. The agrobacteria were collected and resuspended in infection buffer including 10 mM Mes-KOH (pH 5.6) and 10 mM $MgCl_2$. GFP and mCherry fluorescent signals from pavement cells was observed 4 days after the infiltration using a confocal laser microscope (FV10i; Olympus).

**Generation of transgenic plants**

For functional complementation experiments, genomic fragments of the *CST2* gene (about 7 kbps), including 5′ and 3′ noncoding regions including promoter and terminator, were amplified by PCR from WT genomic DNA using primers: 5′-ACGCGTCGACTTCTCACCAACAACGCGATGTATCG-3′ and 5′-ACGCGTCGACTCCTGGTGCAGGATCTTCTTGTACG-3′. The DNA fragment was cloned into the *Sal*I site of the pCAMBIA1300 vector (CAMBIA).

For promoter GUS assay, *GUS* gene was amplified from pCAMBIA1303 vector (CAMBIA) using primes: 5′-ATTCGAAGAAACAACATGTTACGTCCTGTAGAAACCCC-3′ and 5′-AGCAAGAACACAACATCATTGTTTGCCTCCCTGCTG-3′. The DNA fragment was inserted into the site just before the stop codon of the *CST2* gene in the construct for the complementation experiment using the In-Fusion cloning system.

For generation of *CST2* overexpression plants, full length cDNA of *CST2* gene was amplified from cDNAs by PCR using primers: 5′-ACGCGTCGACATGCATCTGATTAATGCGGTGGC-3′ and 5′-ACGCGTCGACTCAGTTGTTTCTTCGAATCGGCTCGG-3′. The cDNA fragment amplified was cloned into the *Sal*I site downstream of 35S promoter of pRI101-AN vector. For overexpression of CST2-GFP in *cbl2 cbl3* double mutant, pRI101-AN containing *CST2-GFP* as described above was used to generate the transgenic plants.

The plasmids constructed as above were transformed into the *Agrobacterium tumefaciens* GV3101 strain. *Agrobacterium* was transformed into the *cst2-1* mutant by the floral dip method [57]. Transgenic plants were selected by resistance against hygromycin or Kanamycin and used for analysis. Transgenic lines were used for phenotypic analysis and observation as described below.

**Phenotypic analysis of transgenic lines**

For analysis of complementation lines, three independent lines (Comp1 to Copm3) lines were grown on soil for 4 weeks and used for comparison of growth, stomatal opening, and photosynthetic electron transfer as described above.

To investigate the genetic interaction of CST2 and CBL2/3, seedlings including *cst2*, *cbl2 cbl3*, and *cbl2 cbl3 cst2-1*, and *CST2-GFP*/ *cbl2 cbl3* were grown in 1/2 MS agar medium for 7 days, then transferred to a new 1/2 MS agar medium with (5 and 10 mM) or without Mg supplementation. Plants were further grown for 2 weeks.

**Promoter-GUS analysis**

Leaves and roots were sampled for 1 to 3-week-old seedling for promoter-GUS assay. The samples were fixed with 90% acetone for 20 min on ice, and then incubated in the GUS staining solution {0.5 mg/ ml 5-bromo-5-chloro-3-indolyl-β-d-glucuronide (X-Gluc), 0.5 mM $K_5[Fe(CN)_6]$, 0.5 mM $K_3[Fe(CN)_6]$, 50 mM sodium phosphate buffer (pH 7.0)} at 37 °C for 14 h. After washed with 70% ethanol and fixed with the solution (15% acetic acid and 85% ethanol), the GUS signal was observed using an upright microscope (Eclipse 50i; Nikon) and a charge-coupled device (CCD) camera (DS-5Mc-L2; Nikon). Tissue sections of the GUS-stained plants were performed as previous method [58]. To make plastic sections, samples were fixed in formalin/acetic acid/alcohol and embedded in Technovit 7100 resin (Heraeus Kulzer; Wehrheim). Then 4-μm sections were prepared and stained with 0.04% neutral red.

**Construction of phylogenetic tree**

Amino acid sequences of CST2 homologs were aligned using MUSCLE [59]. The phylogenetic tree was constructed using the neighbor-joining method and bootstrapping of 1000 replications in MEGAX [60]. Full-length amino acid sequences of CST2 and homolog proteins were used to construct phylogenetic trees.

**Generation of CST2 antibodies**

Anti-CST2 was raised against the recombinant CST2 fragment as an antigen in a rabbit (Medical & Biological Laboratories). The cDNA of CST2 C-terminal fragment (*CST2 C-ter*) was amplified by PCR using primers: 5′ -CGGGATCCACGACAATCATTAGTGGAGCTC-3′ and 5′-CGGGATCCTCAGTTGTTTCTTCGAATCGGCTCGG-3′ and cloned into the *Bam*HI site of the pET30a vector (Novegen). The resulting construct was transformed into the *E. coli* BL21 (DE3) strain. The recombinant CST2 protein was expressed as a fusion protein to the His-tag (His-CST2). The fusion protein was purified using the Profinity IMAC Ni-charged resin (BIO-RAD). The His-CST2 protein was obtained by elution with imidazole and was used to immunize the rabbit as antigens.

**Immunoblotting of CST2 proteins**

Immunoblotting of CST2 was performed with guard and mesophyll cell protoplasts (GCPs and MCPs) isolated from rosette leaves of Arabidopsis plants, as described previously [61]. Proteins were extracted from leaves and roots according to Inoue et al. (2008) [11] and Hayashi et al. (2017) [56]. The protein samples were subjected to SDS-PAGE. Immunoblotting of were performed using the antibodies against CST2, V-PPase, actin. The immunoblotting of CST2 in the leaves of CST2-overexpression lines were similarly performed.

To investigate the effect of high concentration of Mg on CST2 protein expression, WT plants were grown in 1/2 MS agar medium for 2 weeks and then transferred to the 1/2 MS agar medium supplemented with 20 mM Mg. Protein samples were prepared from leaves at the indicated time. In addition, plants were grown in 1/2 MS agar medium containing different Mg concentrations for 2 weeks and the leaves were used for protein sample preparation. These samples were subjected to immunoblotting as described above. Experiments repeated three times on separate occasions gave similar results. Anti-actin (Sigma-Aldrich) and Anti-V-PPase (COSMO BIO) antibodies were purchased.

**In vitro pull-down assay**

Full-length cDNAs of *CIPK26* and *SRK2E* were amplified from the wild-type (Col-0) cDNAs using the primers: 5'-GGTTCCGCGTGGATCCATGAATCGGCCAAAGGTTCAGC-3' and 5'-

GAATTCCCGGGGATCTTATTTGCTTAGACCAGAGCTCTC-3' for *CIPK26* and 5'-GGTTCCGCGTGGATCCATGGATCGACCAGCAGTGAGTGG-3' and 5'-GAATTCCCGGGGATCTCACATTGCGTACACAATCTCTC-3' for *SRK2E*. The amplified products were cloned into pGEX2T vector (GE Healthcare) using In-Fusion cloning system. The resulting constructs were transformed into the *E. coli* BL21 (DE3) strain. The *E. coli* extracts containing a GST-tagged CIPK26 and SRK2E protein and that containing a His-tagged CST2-Cter protein were mixed in equal amounts and added to 0.5% TritonX-100. The mixtures were incubated with 30 µL glutathione-Sepharose 4B (GE Healthcare) for 30 min at 4 °C. GST-tagged proteins were then purified with glutathione-Sepharose 4B from the mixture and washed 3 times with Tris-buffered saline (TBS); boundary matrices were then solubilized by adding 20 µL SDS sample buffer. The solubilized proteins were subjected to SDS-PAGE and immunoblotting was done as described above. Polyclonal antibody against the glutathione-S-transferase (Anti-GST antibody) was used for immunoblotting, as reported previously (Hayashi et al., 2017) [56]. Anti-His tag antibody was purchased. (Wako).

**BiFC assay**

To test the interaction of CST2 with CIPK26 in plant cells, bimolecular fluorescent complementation (BiFC) assay was performed using *N. benthamiana* leaves. Full-length cDNAs of *CST2*, *CIPK26*, and *SRK2E* were amplified by RT-PCR using the following oligonucleotide primers: 5'-GAGGGTACCGCTCCCATGCATCTGATTAATGCGGTGGC-3' and 5'-GTATGGGTACATCCCGTTGTTTCTTCGAATCGGCTCGG-3' for *CST2*, 5'-GAGGGTACCGCTCCCATGAATCGGCCAAAGGTTCAGC-3' and 5'-CTTTTGCTCCATCCCTTTGCTTAGACCAGAGCTCTC-3' and 5'-GAGGGTACCGCTCCCATGAATCGGCCAAAGGTTCAGC-3' and 5'-GTATGGGTACATCCCTTTGCTTAGACCAGAGCTCTC-3' for *CIPK26*, and 5'-GAGGGTACCGCTCCCATGGATCGACCAGCAGTGAGTGG-3' and 5'-CTTTTGCTCCATCCCCATTGCGTACACAATCTCTC-3' for *SRK2E*. Each amplified cDNA was cloned into the *Sma*I site of both binary vectors pSPYNE173 and pSPYCE(M) [62] using the In-Fusion system. The pSPYNE-35S bearing *SRK2E* and pSPYCE-35S vectors bearing *CIPK26* cDNA were used as a positive control [33]. The resulting vectors were introduced into *Agrobacterium tumefaciens* (GV3101). Agrobacteria-mediated co-infiltration of *N. benthamiana* leaves with pSPYNE and pSPYCE containing the indicated inserts was performed as

previously described [16, 62] except that the p19 silencing suppressor strain was mixed and simultaneously infiltrated. Detection of reconstituted YFP fluorescence was monitored 4 days after infiltration using a confocal microscope as described above.

### *In vitro* kinase assay

To test whether the CIPK26 phosphorylates CST2, we performed *in vitro* phosphorylation assay. The plasmid constructs for recombinant proteins, GST-CIPK26 and His-CST2 C-ter as described above were used. To inactivate the kinase activity of CIPK26 for use as a negative control, a mutated protein with a single amino acid substitution CIPK26$^{D154N}$ was used. The aspartic acid is a binding site of $Mg^{2+}$-ATP in protein kinases and substitution of the aspartic acid with asparagine leads to inactivation of protein kinases [11, 63]. Nucleotide substitution was introduced into the *CIPK26* gene in the pGEX2T vector as templates for inverse PCR and self-ligation. Inverse PCR was performed using the oligonucleotide primers 5′-AATTTTGGATTGAGTGCGTTGTCC-3′ and 5′-AGAGACTTTCAGATTTCCTTGAGC-3′. The resulting vector was introduced into the *E. coli* strain BL21 (DE3), and used for protein expression.

The recombinant GST- and His-fused proteins were expressed and purified as described above, and used in the *in vitro* phosphorylation assay. The assay was carried out using a reaction mixture (30 µL) containing 50 mM HEPES-NaOH (pH 7.4), 10 mM $MgCl_2$, 10 mM $MnCl_2$, 10 µM ATP, 5 µCi [γ-$^{32}$P] ATP (PerkinElmer), and 2 µg of each recombinant proteins for 1 h at 25°C. The samples were then subjected to SDS-PAGE and stained with Coomassie Brilliant Blue. Dried gels were exposed to an imaging plate (BAS IP-MS 2040; FUJIFILM) and $^{32}$P incorporation was detected with a Typhoon FLA 7000 Laser Scanner/Imager (GE Healthcare).

### Statistical analysis

All experiments were independently repeated at least two times. Statistical analyses were performed by Tukey's test. Significance of differences were defined as $^{*}P < 0.05$, $^{**}P < 0.01$, $^{***}P < 0.001$, or by different letters ($P < 0.01$).

### Acknowledgements

We thank the NASC for providing seed stocks. We also thank T. Horie (Shinshu Univ.), T. Miyaji, S. Munemasa, and Y. Murata (Okayama Univ.) for discussion,

and T. Shinagawa and A. Kawajiri for technical assistance. This work was supported, in part, by Japan Society for the Promotion of Science (JSPS) (KAKENHI grant nos. 15K07101 and 20K06703 to S.I. and 16H06296 and 21H05034 to JFM), Grants-in-Aid for Scientific Research from MEXT nos. 20H05687 and 20H05910 to T.K., and the Toyoaki Scholarship Foundation (to S.I.).

**Author contributions**

S.I., T.K., and J.F.M. conceived and designed the experiments. S.I., M.H., K.Y., E.G., S.I., M.O., S.H., and T.S. performed the experiments. S.I., M.H., K.Y., T.S., T.K., T.K., and J.F.M. analyzed the data. S.I. and J.F.M. wrote the article. T.K. gave critical comments.

**References**

1. Roelfsema, M.R. & Hedrich, R. In the light of stomatal opening: new insights into 'the Watergate'. *New Phytol.* **167**, 665-691 (2005).
2. Shimazaki, K., Doi, M., Assmann, S. M., & Kinoshita, T. Light regulation of stomatal movement. *Annual review of plant biology*, **58**, 219-247 (2007).
3. Willmer, C. & Fricker, M. Stomata. (Springer Nature Press, 1996)
4. Matthews, J., Vialet-Chabrand, S. & Lawson, T. Role of blue and red light in stomatal dynamic behaviour. *J Exp Bot*. **71***,* 2253-2269 (2020).
5. Tominaga, M., Kinoshita, T. & Shimazaki, K. Guard-cell chloroplasts provide ATP required for $H^+$ pumping in the plasma membrane and stomatal opening. *Plant Cell Physiol*. **42** 795-802 (2001).
6. Suetsugu, N. *et al*. Guard cell chloroplasts are essential for blue light-dependent stomatal opening in Arabidopsis. *PloS one* **9**, e108374 (2014).
7. Santelia, D. & Lawson, T. Rethinking Guard Cell Metabolism. *Plant Physiol*. **172** 1371-1392 (2016).
8. Assmann, S. M. Enhancement of the Stomatal Response to Blue Light by Red Light, Reduced Intercellular Concentrations of $CO_2$, and Low Vapor Pressure Differences. *Plant physiol*. **87**, 226-231 (1988).
9. Zeiger, E. & Hepler, P. K. Light and stomatal function: blue light stimulates swelling of guard cell protoplasts. *Science* **196**, 887-889 (1977).
10. Kinoshita, T. *et al*. Phot1 and phot2 mediate blue light regulation of stomatal opening. *Nature* **414**, 656-60 (2001).

11. Inoue, S. *et al*. Blue light-induced autophosphorylation of phototropin is a primary step for signaling. *Proc Natl Acad Sci USA* **105**, 5626-5631 (2008).
12. Schroeder, J. I., Allen, G. J., Hugouvieux, V., Kwak, J. M. & Waner, D. GUARD CELL SIGNAL TRANSDUCTION. A*nnu Rev Plant Physiol Plant Mol Biol.* **52**, 627-658 (2001).
13. Lebaudy, A. *et al*. Heteromeric $K^+$ channels in plants. *Plant J*. **54**, 1076-1082 (2008).
14. Marten, I., Deeken, R., Hedrich, R. & Roelfsema, M.R. (2010) Light-induced modification of plant plasma membrane ion transport. *Plant Biol.* **12** (s1), 64-79.
15. Zhao, X., Qiao, X., Yuan, J., Ma, X. & Zhang, X. Nitric oxide inhibits blue light-induced stomatal opening by regulating the $K^+$ influx in guard cells. *Plant Sci.* **184**, 29-35 (2012).
16. Inoue, S. *et al*. CIPK23 regulates blue light-dependent stomatal opening in *Arabidopsis thaliana*. *Plant J*. **104**, 679-692 (2020).
17. Jossier, M. *et al*. The Arabidopsis vacuolar anion transporter, AtCLCc, is involved in the regulation of stomatal movements and contributes to salt tolerance. *Plant J*. **64**, 563-576 (2010).
18. De Angeli, A., Zhang, J., Meyer, S. & Martinoia, E. AtALMT9 is a malate-activated vacuolar chloride channel required for stomatal opening in Arabidopsis. *Nat Commun*. **4**, 1804 (2013).
19. Andrés, Z. *et al*. Control of vacuolar dynamics and regulation of stomatal aperture by tonoplast potassium uptake. *Proc Natl Acad Sci U S A*. **111**, E1806-E1814 (2014).
20. Eisenach, C. & De Angeli, A. Ion transport at the vacuole during stomatal movements. *Plant Physiol.* **174**, 520-530 (2017).
21. Inoue, S., Takemiya, A. & Shimazaki, K. Phototropin signaling and stomatal opening as a model case. *Curr Opin Plant Biol*, **13**, 587-593 (2010).
22. Horrer, D. *et al*. Blue light induces a distinct starch degradation pathway in guard cells for stomatal opening. *Curr Biol*. **8**, 362-370 (2016).
23. Flütsch, S. *et al*. Guard cell starch degradation yields glucose for rapid stomatal opening in Arabidopsis. *Plant Cell*. **32**, 2325-2344 (2020).
24. Inoue, S. I. *et al*. Brassinosteroid involvement in *Arabidopsis thaliana* stomatal opening. *Plant Cell Physiol.* **58,** 1048-1058 (2017).
25. Gibson, M. M., Bagga, D. A., Miller, C. G. & Maguire M. E. Magnesium transport in *Salmonella typhimurium*: the influence of new mutations

conferring $Co^{2+}$ resistance on the CorA $Mg^{2+}$ transport system. *Mol Microbiol.* **5,** 2753-2762 (1991).
26. Armitano, J., Redder, P., Guimarães, V. A. & Linder, P. An Essential Factor for High $Mg^{2++}$ Tolerance of *Staphylococcus aureus*. *Front Microbiol*. **7**, 1888 (2016).
27. Trachsel, E., Redder, P., Linder, P. & Armitano, J. Genetic screens reveal novel major and minor players in magnesium homeostasis of *Staphylococcus aureus*. *PLoS genetics*. **15,** e1008336 (2019).
28. Chen, Y.S. *et al.* Crystal structure of an archaeal CorB magnesium transporter. *Nat Commun*. **12**, 4028 (2021).
29. Arjona, F. J. & de Baaij, J. CrossTalk opposing view: CNNM proteins are not $Na^+$ /$Mg^{2+}$ exchangers but $Mg^{2+}$ transport regulators playing a central role in transepithelial $Mg^{2+}$ reabsorption. *J Physiol*. **596**, 747-750 (2018).
30. Funato, Y., Furutani, K., Kurachi, Y. & Miki, H. CrossTalk proposal: CNNM proteins are $Na^+$ /$Mg^{2+}$ exchangers playing a central role in transepithelial $Mg^{2+}$ reabsorption. *J Physiol*. **596**, 743-746 (2018).
31. Yang, M., Jensen, L. T., Gardner, A. J. & Culotta, V. C. (2005). Manganese toxicity and Saccharomyces cerevisiae Mam3p, a member of the ACDP (ancient conserved domain protein) family. *Biochem J*. **386**, 479-487 (2005).
32. Tang, R.J. *et al*. Tonoplast CBL-CIPK calcium signaling network regulates magnesium homeostasis in Arabidopsis. *Proc Natl Acad Sci U S A*. **112**, 3134-3139 (2015).
33. Mogami, J. *et al*. Two distinct families of protein kinases are required for plant growth under high external $Mg^{2+}$ concentrations in Arabidopsis. *Plant Physiol*. **167**, 1039-1057 (2015).
34. Inoue, S. I. & Kinoshita, T. Blue Light Regulation of Stomatal Opening and the Plasma Membrane $H^+$-ATPase. *Plant Physiol.* **174**, 531–538 (2017).
35. Huber, S. C. & Maury, W. Effects of Magnesium on Intact Chloroplasts: I. EVIDENCE FOR ACTIVATION OF (SODIUM) POTASSIUM/PROTON EXCHANGE ACROSS THE CHLOROPLAST ENVELOPE. *Plant Physiol*. **65**, 350-354 (1980).
36. Wu et al. 1991 Surface charge-mediated efects of $Mg^{2+}$ on $K^+$ flux across the chloroplast envelope are associated with regulation of stromal pH and photosynthesis. *Plant Physiol*. **97**, 580-587 (1991).

37. Kuromori, T., Seo, M. & Shinozaki, K. ABA Transport and Plant Water Stress Responses. *Trends Plant Sci*. **23**, 513-522 (2018).
38. Tang, R.J. & Luan, S. Regulation of calcium and magnesium homeostasis in plants: from transporters to signaling network. *Curr Opin Plant Biol*. **39**, 97-105 (2017).
39. Chen, Z. C., Peng, W. T., Li, J. & Liao, H. Functional dissection and transport mechanism of magnesium in plants. *Semin. Cell Dev. Biol.* **74**, 142-152 (2018).
40. Li, L., Tutone, A.F., Drummond, R.S., Gardner, R.C. & Luan, S. A novel family of magnesium transport genes in *Arabidopsis*. *Plant Cell* **13**, 2761-2775 (2001)
41. Saito, T. *et al*. Expression and functional analysis of the CorA-MRS2-ALR-type magnesium transporter family in rice. *Plant Cell Physiol*. **54,** 1673-1683 (2013).
42. Mao, D. *et al*. Arabidopsis transporter MGT6 mediates magnesium uptake and is required for growth under magnesium limitation. *Plant Cell* **26**, 2234-2248 (2014).
43. Sun, Y., Yang, R., Li, L. & Huang, J. The magnesium transporter MGT10 is essential for chloroplast development and photosynthesis in *Arabidopsis thaliana*. *Mol Plant* **10**, 1584-1587 (2017).
44. Li, J. *et al*. Diel magnesium fluctuations in chloroplasts contribute to photosynthesis in rice. *Nat Plants* **4,** 690-698 (2020).
45. Conn, S. J. *et al*. Magnesium transporters, MGT2/MRS2-1 and MGT3/MRS2-5, are important for magnesium partitioning within *Arabidopsis thaliana* mesophyll vacuoles. *New Phytol*. **190**, 583-594 (2011).
46. Shaul, O. *et al*. Cloning and characterization of a novel $Mg^{2+}/H^{+}$ exchanger. *EMBO J*. **18**, 3973-3980 (1999).
47. Gao, C., Zhao, Q. & Jiang, L. Vacuoles protect plants from high magnesium stress. *Proc Natl Acad Sci U S A*. **112**, 2931-2932 (2015).
48. Yamazaki, D. *et al*. Basolateral $Mg^{2+}$ extrusion via CNNM4 mediates transcellular $Mg^{2+}$ transport across epithelia: a mouse model. *PLoS Genet*. **9**, e1003983 (2013).
49. Norén, H., Svensson, P. & Andersson, B. A convenient and versatile hydroponic cultivation system for *Arabidopsis thaliana*. *Physiol Plant.* **121,** 343–348 (2004).

50. Yamaji N. *et al.* Reducing phosphorus accumulation in rice grains with an impaired transporter in the node. *Nature* 541, 92–95 (2017).
51. de Carbonnel, M. *et al*. The Arabidopsis PHYTOCHROME KINASE SUBSTRATE 2 protein is a phototropin signaling element that regulates leaf flattening and leaf positioning. *Plant Physiol.* **152,** 1391–1405 (2010).
52. Doi, M., Shigenaga, A., Emi, T., Kinoshita, T. & Shimazaki, K. A transgene encoding a blue-light receptor, phot1, restores blue-light responses in the Arabidopsis *phot1 phot2* double mutant. *J Exp Bot.* **55,** 517–523 (2004).
53. Gotoh, E., Oiwamoto, K., Inoue, S., Shimazaki, K., & Doi, M. Stomatal response to blue light in crassulacean acid metabolism plants *Kalanchoe pinnata* and *Kalanchoe daigremontiana*. *J Exp Bot.* **70,** 1367-1374 (2019).
54. Suzuki, T. *et al*. Development of the Mitsucal computer system to identify causal mutation with a high-throughput sequencer. *Plant Reprod.* **31,** 117-128 (2018).
55. Mumberg, D., Müller, R. & Funk, M. Yeast vectors for the controlled expression of heterologous proteins in different genetic backgrounds. *Gene* **156,** 119-122 (1995).
56. Hayashi, M., Inoue, S., Ueno, Y. & Kinoshita, T. A Raf-like protein kinase BHP mediates blue light-dependent stomatal opening. *Sci Rep.* **7,** 45586 (2017).
57. Clough, S.J. & Bent, A.F. Floral dip: a simplified method for Agrobacterium-mediated transformation of *Arabidopsis thaliana*. *Plant J.* **16,** 735-43 (1998).
58. Uchida, N. *et al.* Regulation of inflorescence architecture by intertissue layer ligand-receptor communication between endodermis and phloem. *Proc Natl Acad Sci U S A*. **109**, 6337-6342 (2012).
59. Edgar, R.C. MUSCLE: multiple sequence alignment with high accuracy and high throughput. *Nucleic Acids Res.* **32,** 1792-1797 (2004).
60. Kumar, S., Stecher, G., Li, M., Knyaz, C. & Tamura, K. MEGA X: molecular evolutionary genetics analysis across computing platforms. *Mol Biol Evol.* **35,** 1547-1549 (2018).
61. Ueno, K., Kinoshita, T., Inoue, S., Emi, T. & Shimazaki, K. Biochemical characterization of plasma membrane $H^+$-ATPase activation in guard cell protoplasts of *Arabidopsis thaliana* in response to blue light. *Plant Cell Physiol.* **46,** 955-963 (2005).

62. Walter, M. *et al.* Visualization of protein interactions in living plant cells using bimolecular fluorescence complementation. *Plant J.* **40,** 428-438 (2004).
63. Hanks, S. K. & Hunter, T. Protein kinases 6. The eukaryotic protein kinase superfamily: kinase (catalytic) domain structure and classification. *FASEB J* **9,** 576-596 (1995).

## Figure Legends

**Figure 1. Isolation and physiological characterization of *cst2* mutants**

**a,** Infrared thermal images of Arabidopsis WT and *cst2-1* plants during growth under light. Plants were grown for 3 weeks.

**b,** Light-dependent stomatal opening in WT and *cst2* mutants. Epidermal fragments were isolated from dark-adapted plants and irradiated with mixed light (red light: 50 µmol $m^{-2}$ $s^{-1}$ and blue light: 10 µmol $m^{-2}$ $s^{-1}$) for 3 h. Data represent the mean ± SD of triplicate experiments. Each experiment used 30 stomata. Asterisks indicate statistically significant differences from the corresponding WT control using Two-way ANOVA by Tukey's multiple comparisons test (*$P < 0.05$, ***$P < 0.001$).

**c**, Photosynthetic activity of WT and *cst2* mutants. Quantum yield of electron transfer to PSII (ΦPSII) was measured in WT, *cst2-1*, *cst2-2* and complementation line #1 (comp1) grown under 200 µmol $m^{-2}$ $s^{-1}$ for 5 weeks. Measurement was made after exposure of leaves to actinic light of 200 µmol $m^{-2}$ $s^{-1}$ for 5 min. Left panel, image of ΦPSII and right panel, photosynthetic activity. Data are means ± SD (n = 3). Asterisks indicate statistically significant differences from the corresponding WT control using One-way ANOVA by Dunnett's multiple comparisons test (***$P < 0.001$).

**d**, Phenotype (left) and fresh weight (right) of WT and *cst2* mutants grown on soil. Plants were grown for 4 weeks. Data are means ± SD (n = 20). Asterisks indicate statistically significant differences from the corresponding WT control using One-way ANOVA by Dunnett's multiple comparisons test (***$P < 0.001$).

**e,** Effects of drought stress on the growth of WT and *cst2-1*. Plants were grown under well-watered conditions for 24 d, and then subjected to drought stress for 16 d without watering.

**Figure 2. Mg transport activity, subcellular localization and expression pattern of CST2**

**a,** Mg concentration in transgenic yeast cells. Yeast mutant (*mam3*) expressing *MAM3*, *CST2* cDNA or empty vector was grown in SD medium containing 3 mM Mg for 14 h. Mg concentration in yeast was determined by ICP-MS. Data represent the mean ± SD (n = 5). Asterisks indicate statistically significant differences from the empty vector/WT using One-way ANOVA by Dunnett's multiple comparisons test (** $P < 0.01$, *** $P < 0.001$).

**b,** Subcellular localization of CST2-GFP. CST2-GFP was expressed alone (left) or co-expressed with Tonoplast target signal (TTS)-mCherry (center) or with mCherry-AHA1 (right) in leaf epidermal cells of *Nicotiana benthamiana*. Fluorescent images were obtained using a confocal laser microscope.

**c,** Expression pattern of *CST2* in different organs. Plants were exposed to a nutrient solution containing 0, 0.4 and 5 mM Mg for 2 d and the roots and leaves were sampled for RNA expression. Expression relative to –Mg roots is shown. Data are means± SD (n = 4). Different letters indicate significant differences at $P < 0.01$ by Tukey-Kramer's test.

**d,** Time-dependent change of CST2 protein in response to high Mg concentration. WT Plants were grown on 1/2 MS containing agar medium for 2 weeks, and then transferred to the 1/2 MS medium with 20 mM Mg. Proteins were extracted at the indicated time points and subjected to immunoblotting using CST2 and V-PPase antibodies. **e,** Mg concentration-dependent CST2 protein expression. Plants were grown on 1/2 MS containing agar medium containing different Mg concentrations for 2 weeks. Immunoblotting was performed as in d.

**Figure 3. Tissue-specificity of *CST2* expression**

**a-i**, Expression pattern of *CST2* gene in different organs and tissues. Transgenic plants carrying *CST2* promoter-*GUS* were grown on 1/2 MS containing agar medium and used for GUS assay. (**a**) A young one-week-old plant. (**b**) A three-week-old plant. (**c**) Cotyledon. (**d**) Magnified image of cotyledon. (**e**) Magnified image of leaf surface of a true leaf. (**f**) Root. (**g**) Primary root tip. (**h**,**i**) Cross section of a true leaf (**h**) and the primary root (**i**). Red color shows cell wall stained by Nile red.

**j,** Expression of CST2 protein in different cells and tissues. WT Plants were grown on soil for 4 weeks, and different cell types were isolated. GCPs; guard cell

protoplasts. MCPs; mesophyll cell protoplasts. Immunoblotting was performed using antibodies against CST2, V-PPase, and actin.

**Figure 4. Phenotypic characterization of *cst2* mutants in relation to different Mg concentrations**

**a**, Growth of WT and *cst2-1* in hydroponic medium. Plants were grown in a solution containing 0.25 mM, 1 mM or 5 mM Mg for 5 weeks.

**b and c,** Dry weight of shoot (**e**) and root (**f**) of WT and *cst2* plants grown in hydroponic solution with different Mg concentrations. Data represent the mean ± SD (n = 16). Asterisks indicate statistically significant differences from the corresponding WT control using Two-way ANOVA by Tukey's multiple comparisons test (*$P < 0.05$, **$P < 0.01$, ***$P < 0.001$).

**d**, Shoot Mg concentration in WT, *cst2-1*, and *cst2-2*. The plants were grown on 1/2 MS containing agar medium with or without 5 mM Mg supply. Data represent the mean ± SD (n = 6). Asterisks indicate statistically significant differences from the corresponding WT control using Two-way ANOVA by Tukey's multiple comparisons test (***$P < 0.001$).

**Figure 5. Time-dependent change of stomatal opening in response to high Mg**

**a,** Light- and Mg-dependent stomatal opening in WT and *cst2* mutant. Plants were grown in hydroponic medium containing various Mg concentrations for 28-32 days. Epidermal fragments were isolated from dark-adapted plants and irradiated by the mixed light for 3 h as described in Figure 1b. Data represent the mean ± SD of 3-5 experiments. Each experiment used 30 stomata. Asterisks indicate statistically significant differences from the corresponding WT control using Two-way ANOVA by Tukey's multiple comparisons test (*$P < 0.05$, **$P < 0.01$, ***$P < 0.001$).

**b,** Time-course of stomatal opening capacities of WT and *cst2* mutants in response to high Mg treatment. Plants were grown hydroponically in 0.2 mM Mg conditions for 4 weeks, followed by transferring to 5 mM Mg. Rosette leaves were harvested 3 h after the start of the light period. Epidermal fragments were immediately isolated and stomatal apertures were determined by microscopy. Data represent the mean ± SD of 4 experiments. Each experiment used 30 stomata. Asterisks indicate statistically significant differences from corresponding

WT control using Two-way ANOVA by Tukey's multiple comparisons test (*$P$ < 0.05, ***$P$ < 0.001).

**c and d,** Changes in stomatal conductance (**c**) and photosynthetic rate (**d**) in response to light in leaves of WT and *cst2* mutants. Plants were grown for 5 d in 5 mM Mg solution, followed by maintaining in the dark overnight prior to measurements at the fifth day morning. White light at 1000 µmol $m^{-2}$ $s^{-1}$ was applied to the upper surface of a leaf. Experiments repeated on two occasions gave similar results.

**Figure 6. Genetic and physical interaction between CST2 and CBL-CIPK.**

**a**, Growth of WT, *cst2-1*, *cbl2 cbl3*, *cbl2 cbl3 cst2-1* (left), and shoot fresh weight (right) of the plants at different Mg concentrations. Asterisks indicate statistically significant differences using Two-way ANOVA by Tukey's multiple comparisons test (*$P$ < 0.05, **$P$ < 0.01, ***$P$ < 0.001). Asterisks just on each error bar show significant differences comparison with corresponding WT control. **b,** Growth of WT, *cst2-1*, *cbl2 cbl3*, *CST2-GFP*/*cbl2 cbl3* lines (#2, #5, #8) (left), and shoot fresh weight (right) of the plants at different Mg concentrations. Plants were grown in 1/2 MS containing agar medium for 7 d and then transferred to a new 1/2 MS containing agar medium with or without Mg supply at indicated concentrations. Plants were further grown for 2 weeks. Data represent the mean ± SD (n = 22-32 for (**a**) and n = 21-34 for (**b**)). Asterisks indicate statistically significant differences from WT control using Two-way ANOVA by Tukey's multiple comparisons test (**$P$ < 0.01, ***$P$ < 0.001).

**c**, *In vitro* pull-down assay for the interaction of CST2 with CIPK26. Recombinant GST-CIPK26, GST-SRK2E, and His-CST2 C-terminal region (CST2 C-ter) were expressed in *E. coli*. Extract from the *E. coli* cells expressing GST-CIPK26 or GST-SRK2E was mixed with that expressing His-CST2 C-ter and reacted with glutathione-Sepharose 4B beads. The proteins on the beads were subjected to SDS-PAGE and then immunoblotted using anti-GST and anti-His antibodies.

**d**, *In vivo* interaction of CST2 with CIPK26 determined by a bimolecular fluorescence complementation (BiFC) assay. CIPK26, SRK2E, CST2 constructs were co-transformed with indicated combinations into *Nicotiana benthamiana* leaves. The reconstituted fluorescent signal was observed using a confocal laser microscope. Co-expression of SRK2E with CIPK26 is a positive control. nYFP and cYFP represent the N- and C-terminal halves of the YFP protein, respectively.

**e**, *In vitro* phosphorylation of CST2 by CIPK26. Autoradiograph (left) and CBB stain (right) of gel were shown. CST2 C-ter was reacted with WT GST-CIPK26 or kinase dead (K.D.) GST-CIPK26 in the presence of $P^{32}$ ATP to detect the CIPK26-mediated phosphorylation.

**Figure 7. Schematic presentation of CST2 role in stomatal opening**

Mg concentration in cytosol of stomatal guard cells is maintained at a steady level by different ways. One of them is to sequester Mg into vacuole by CST2 localized at the tonoplast to maintain Mg homeostasis, which is important for stomatal opening (left). Knockout of CST2 results in stomatal closure due to high Mg in the cytosol in the guard cells (right). CST2 is phosphorylated by CBL-CIPK26 for its activation.

**Supplementary Figure 1. Gene mapping, structure and complementation test**

a, Genomic structure of the *CST2* gene. Position of the *cst2-1* mutation and the site of T-DNA insertion in *cst2-2* (GABI_322H07) are indicated. Boxes and lines represent exons and introns, respectively. T-DNA was inserted in the fifth exon for *cst2-2*.

**b,** Expressions of CST2 protein in rosette leaves of WT and *cst2* mutants. Immunoblotting was performed.

**c and d,** Complementation of growth defect (**c**) and impairment stomatal opening (**d**) in the *cst2-1* mutant with a wild-type genomic *CST2* gene. WT, *cst2-1* and *cst2-1* plants harboring a transgene with the WT *CST2* gene (Comp1 to 3) were grown on soil for 4 weeks. Light-dependent stomatal opening was measured as described in Figure 1b. Data represent the mean ± SD of triplicate experiments. Each experiment used 30 stomata. Asterisks indicate statistically significant differences from WT control using Two-way ANOVA by Tukey's multiple comparisons test (***$P < 0.001$).

**e,** Expression of *CST2* in rosette leaves of WT and *cst2-2* plants. RT–PCR analysis was performed. *TUB2* was used as an internal control.

**Supplementary Figure 2. Structure and phylogenetic tree of CST2.**

**a,** Schematic representation of the CST2 protein. CST2 protein has a DUF21 and CBS-pair domains.

**b and c,** Phylogenetic relationships between CST2 and homologous proteins from Arabidopsis thaliana (**b**) and from other organisms (**c**). The alignment was performed using the MUSCLE with full length amino acid sequences. The tree was constructed using MEGAX software with the neighbor-joining method. The Arabidopsis CST2 is shown in bold red letters. Yeast MAM3 is shown in bold letters. The numbers next to the branches are bootstrap values (1,000 replicates). The scale bar represents 0.05 (**b**) or 0.2 (**c**) substitutions per site.

**Supplementary Figure 3. Growth of wild type (WT) and *cst2* mutants grown under different ionic stress conditions**

Plants were grown in 1/2 MS containing agar medium for 7 days and then transferred to a new 1/2 MS containing agar medium containing different ions as indicated for a further 2-weeks.

**Supplementary Figure 4. Growth response of CST2-overexpressing plants to high Mg**

**a,** Expressions level of CST2 protein in rosette leaves of WT and the overexpression lines (OE4 and OE6). Immunoblotting was performed.

**b,** Mg concentration-dependent growth of WT, *cst2-1* mutant, and CST2 overexpressing lines (OE4 and OE6). Plants were grown on 1/2 MS containing agar medium containing different Mg concentrations. After 22 days growth, the plants were photographed and the shoot fresh weight was recorded. Data represent the mean ± SD (n = 10-25). Asterisks indicate statistically significant differences from WT control using Two-way ANOVA by Tukey's multiple comparisons test (*$P < 0.05$, ***$P < 0.001$).

Figure 1

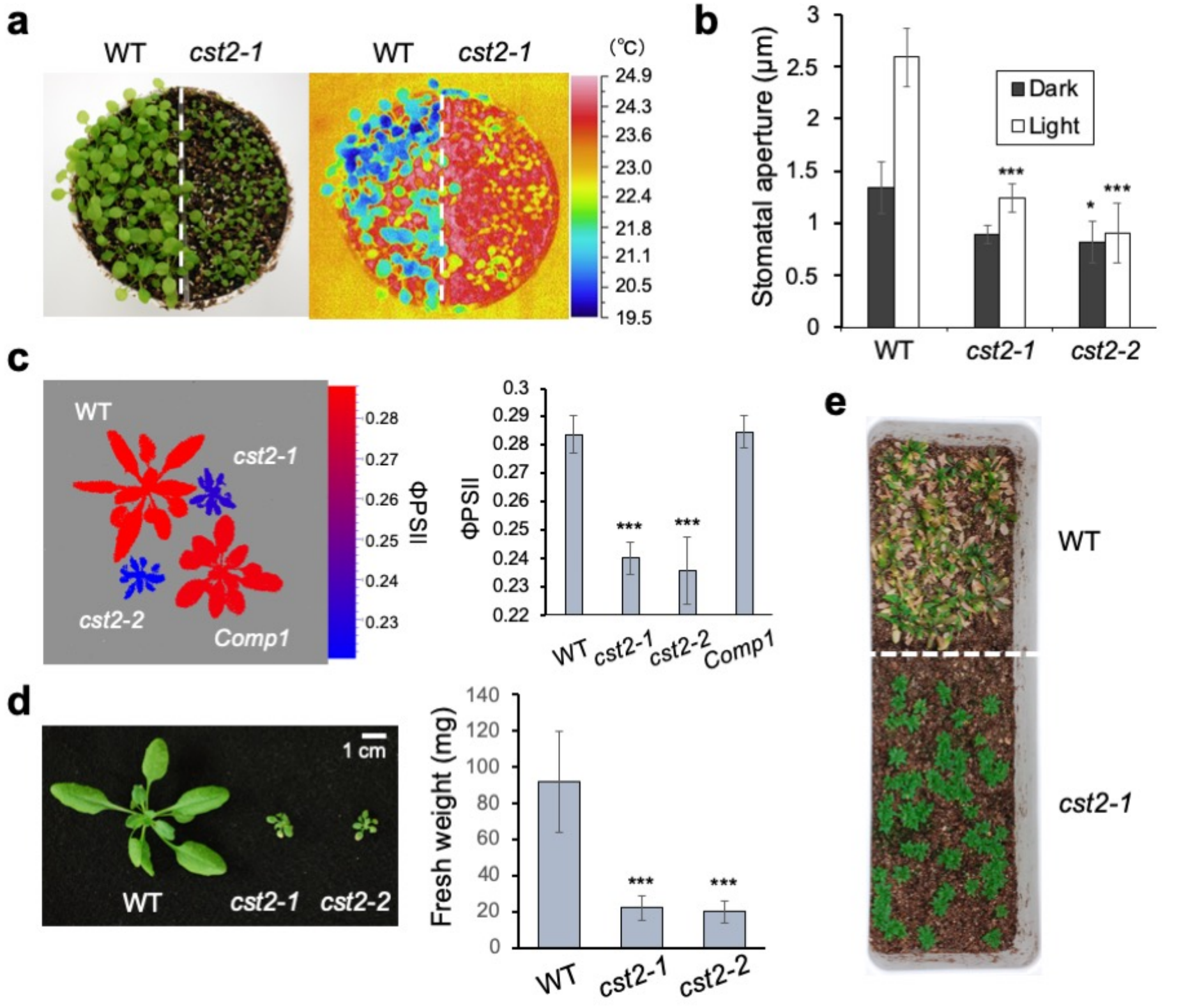


**Figure 1. Isolation and physiological characterization of *cst2* mutants**

**a,** Infrared thermal images of Arabidopsis WT and *cst2-1* plants during growth under light. Plants were grown for 3 weeks.

**b,** Light-dependent stomatal opening in WT and *cst2* mutants. Epidermal fragments were isolated from dark-adapted plants and irradiated with mixed light (red light: 50 μmol $m^{-2}$ $s^{-1}$ and blue light: 10 μmol $m^{-2}$ $s^{-1}$) for 3 h. Data represent the mean ± SD of triplicate experiments. Each experiment used 30 stomata. Asterisks indicate statistically significant differences from the corresponding WT control using Two-way ANOVA by Tukey's multiple comparisons test (*P < 0.05, ***P < 0.001).

**c**, Photosynthetic activity of WT and *cst2* mutants. Quantum yield of electron transfer to PSII (ΦPSII) was measured in WT, *cst2-1*, *cst2-2* and complementation line #1 (comp1) grown under 200 μmol $m^{-2}$ $s^{-1}$ for 5 weeks. Measurement was made after exposure of leaves to actinic light of 200 μmol $m^{-2}$ $s^{-1}$ for 5 min. Left panel, image of ΦPSII and right panel, photosynthetic activity. Data are means ± SD (n = 3). Asterisks indicate statistically significant differences from the corresponding WT control using One-way ANOVA by Dunnett's multiple comparisons test (***P < 0.001).

**d**, Phenotype (left) and fresh weight (right) of WT and *cst2* mutants grown on soil. Plants were grown for 4 weeks. Data are means ± SD (n = 20). Asterisks indicate statistically significant differences from the corresponding WT control using One-way ANOVA by Dunnett's multiple comparisons test (***P < 0.001).

**e,** Effects of drought stress on the growth of WT and *cst2-1*. Plants were grown under well-watered conditions for 24 d, and then subjected to drought stress for 16 d without watering.

Figure 2

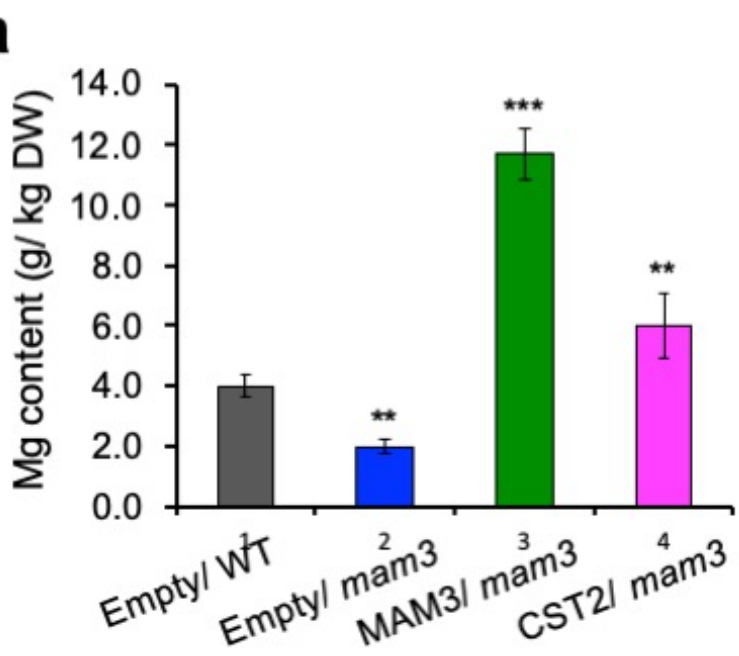


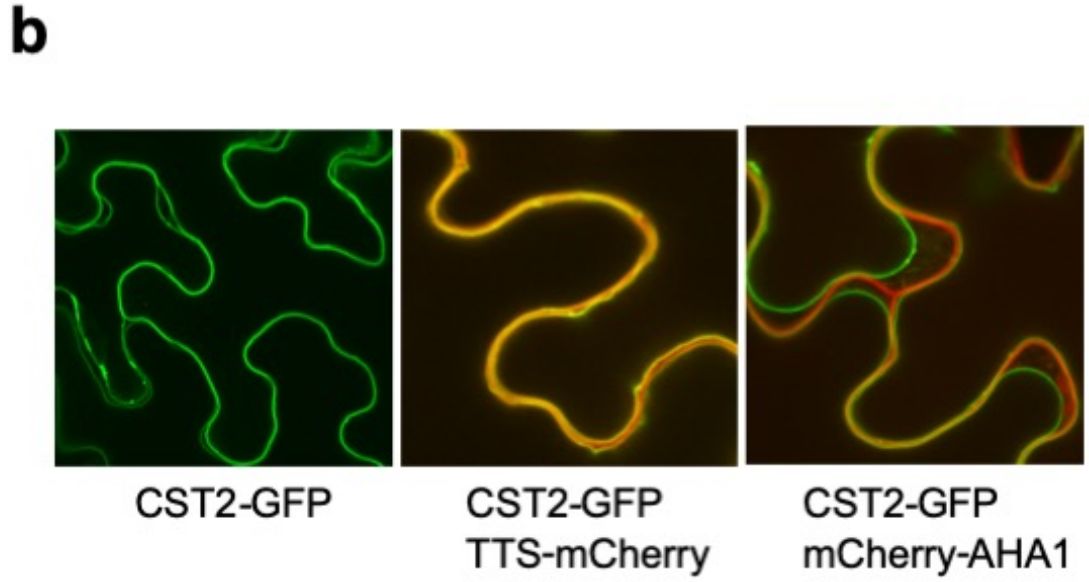


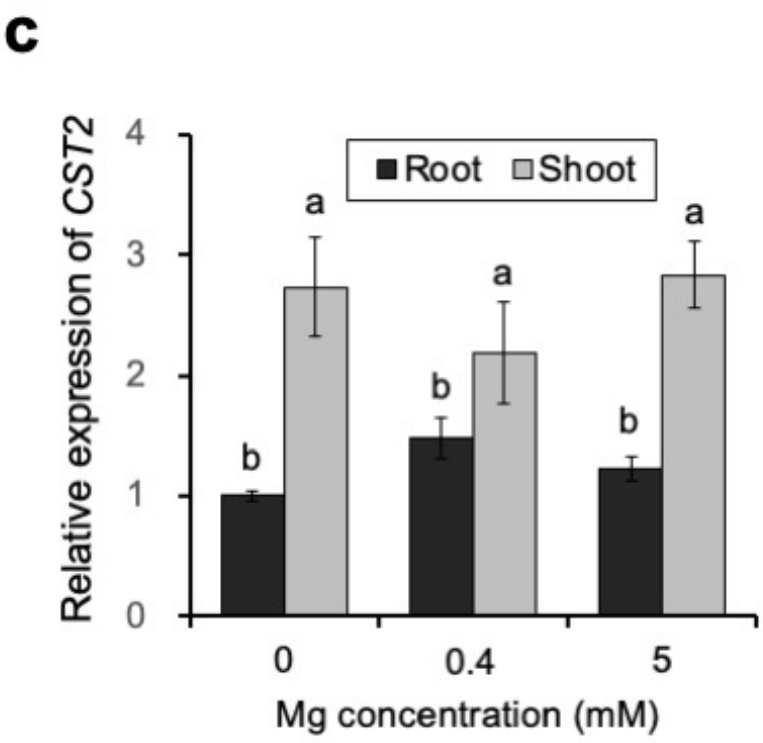


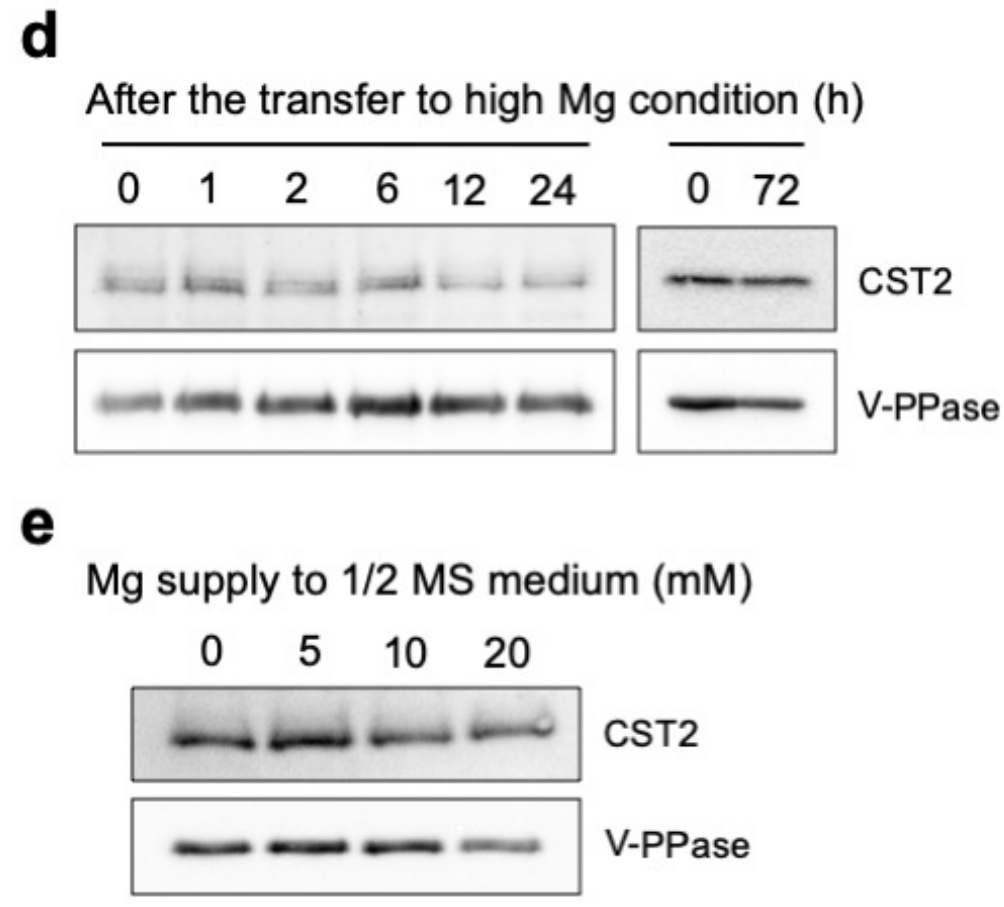


**Figure 2. Mg transport activity, subcellular localization and expression pattern of CST2**
a, Mg concentration in transgenic yeast cells. Yeast mutant (mam3) expressing MAM3, CST2 cDNA or empty vector was grown in SD medium containing 3 mM Mg for 14 h. Mg concentration in yeast was determined by ICP-MS. Data represent the mean ± SD (n = 5). Asterisks indicate statistically significant differences from the empty vector/WT using One-way ANOVA by Dunnett's multiple comparisons test (**P < 0.01, ***P < 0.001).
b, Subcellular localization of CST2-GFP. CST2-GFP was expressed alone (left) or co-expressed with Tonoplast target signal (TTS)-mCherry (center) or with mCherry-AHA1 (right) in leaf epidermal cells of *Nicotiana benthamiana*. Fluorescent images were obtained using a confocal laser microscope.
**c,** Expression pattern of CST2 in different organs. Plants were exposed to a nutrient solution containing 0, 0.4 and 5 mM Mg for 2 d and the roots and leaves were sampled for RNA expression. Expression relative to –Mg roots is shown. Data are means± SD (n = 4). Different letters indicate significant differences at P < 0.01 by Tukey-Kramer's test.
**d,** Time-dependent change of CST2 protein in response to high Mg concentration. WT Plants were grown on 1/2 MS containing agar medium for 2 weeks, and then transferred to the 1/2 MS medium with 20 mM Mg. Proteins were extracted at the indicated time points and subjected to immunoblotting using CST2 and V-PPase antibodies. **e,** Mg concentration-dependent CST2 protein expression. Plants were grown on 1/2 MS containing agar medium containing different Mg concentrations for 2 weeks. Immunoblotting was performed as in d.

Figure 3

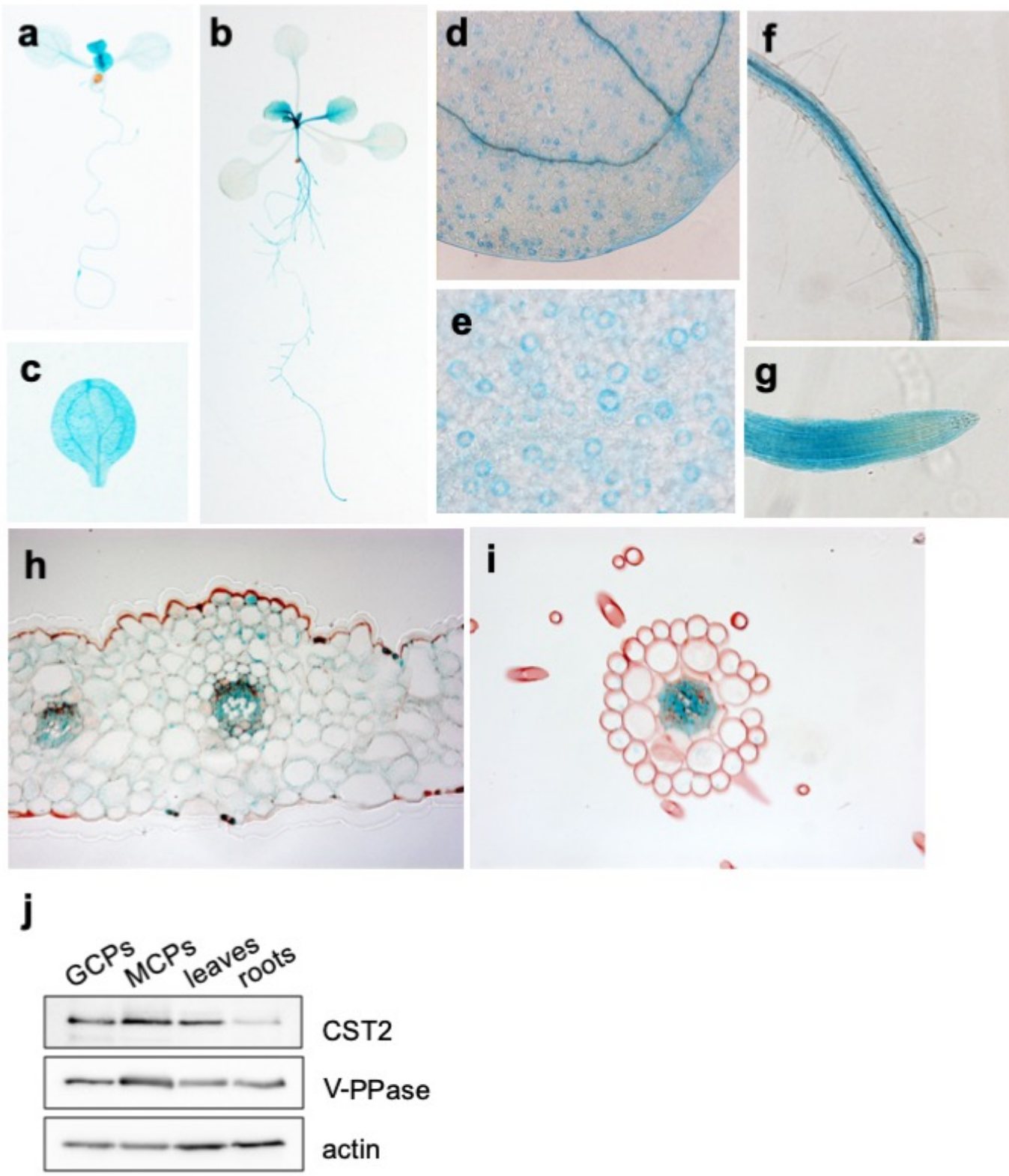


**Figure 3. Tissue-specificity of *CST2* expression**

**a-i**, Expression pattern of *CST2* gene in different organs and tissues. Transgenic plants carrying *CST2* promoter-*GUS* were grown on 1/2 MS containing agar medium and used for GUS assay. (**a**) A young one-week-old plant. (**b**) A three-week-old plant. (**c**) Cotyledon. (**d**) Magnified image of cotyledon. (**e**) Magnified image of leaf surface of a true leaf. (**f**) Root. (**g**) Primary root tip. (**h**,**i**) Cross section of a true leaf (**h**) and the primary root (**i**). Red color shows cell wall stained by Nile red.

**j**, Expression of CST2 protein in different cells and tissues. WT Plants were grown on soil for 4 weeks, and different cell types were isolated. GCPs; guard cell protoplasts. MCPs; mesophyll cell protoplasts. Immunoblotting was performed using antibodies against CST2, V-PPase, and actin.

Figure 4

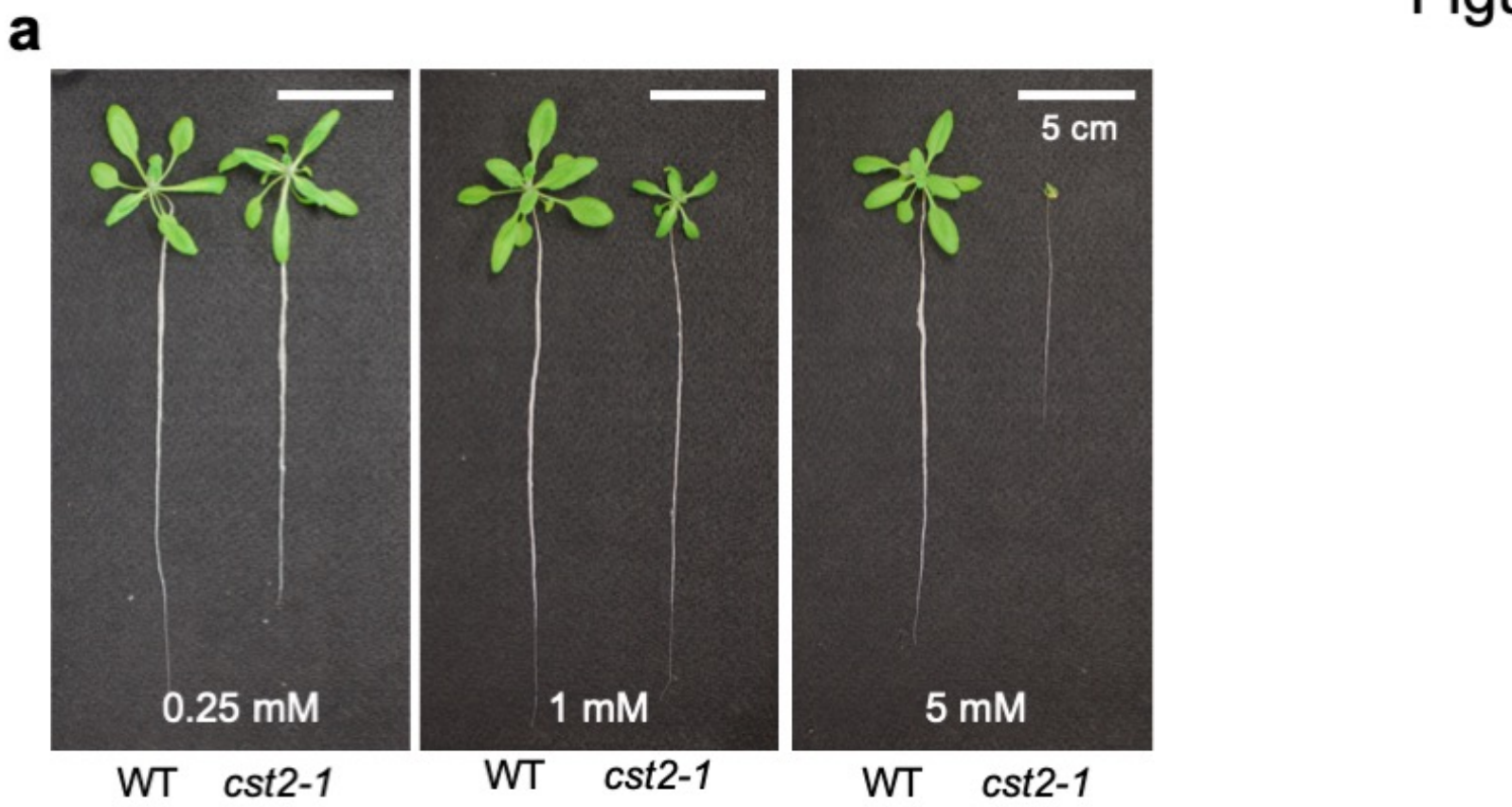


**Figure 4. Phenotypic characterization of *cst2* mutants in relation to different Mg concentrations**

**a**, Growth of WT and *cst2-1* in hydroponic medium. Plants were grown in a solution containing 0.25 mM, 1 mM or 5 mM Mg for 5 weeks.

**b and c,** Dry weight of shoot (**e**) and root (**f**) of WT and *cst2* plants grown in hydroponic solution with different Mg concentrations. Data represent the mean ± SD (n = 16). Asterisks indicate statistically significant differences from the corresponding WT control using Two-way ANOVA by Tukey's multiple comparisons test (*P < 0.05, **P < 0.01, ***P < 0.001).

**d**, Shoot Mg concentration in WT, *cst2-1*, and *cst2-2*. The plants were grown on 1/2 MS containing agar medium with or without 5 mM Mg supply. Data represent the mean ± SD (n = 6). Asterisks indicate statistically significant differences from the corresponding WT control using Two-way ANOVA by Tukey's multiple comparisons test (***P < 0.001).

Figure 5

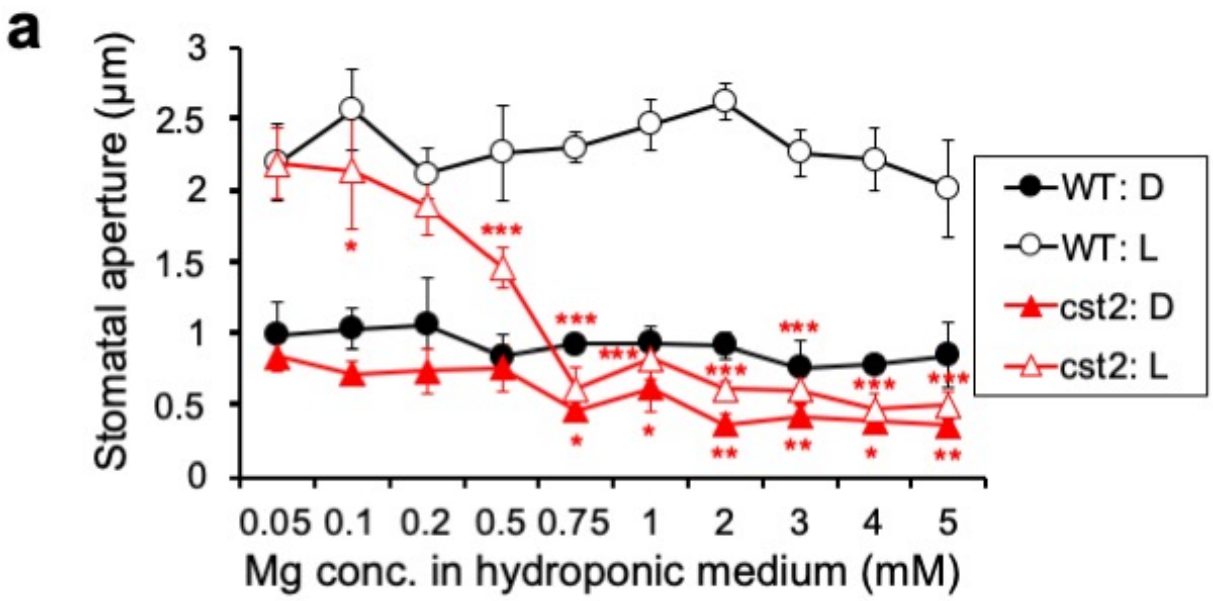


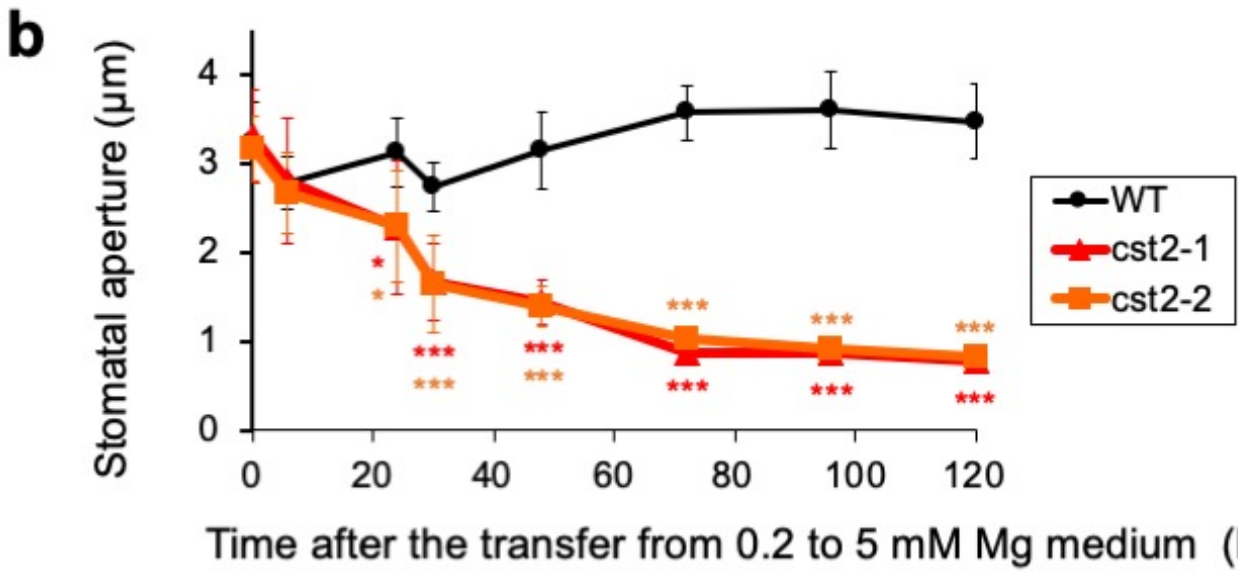


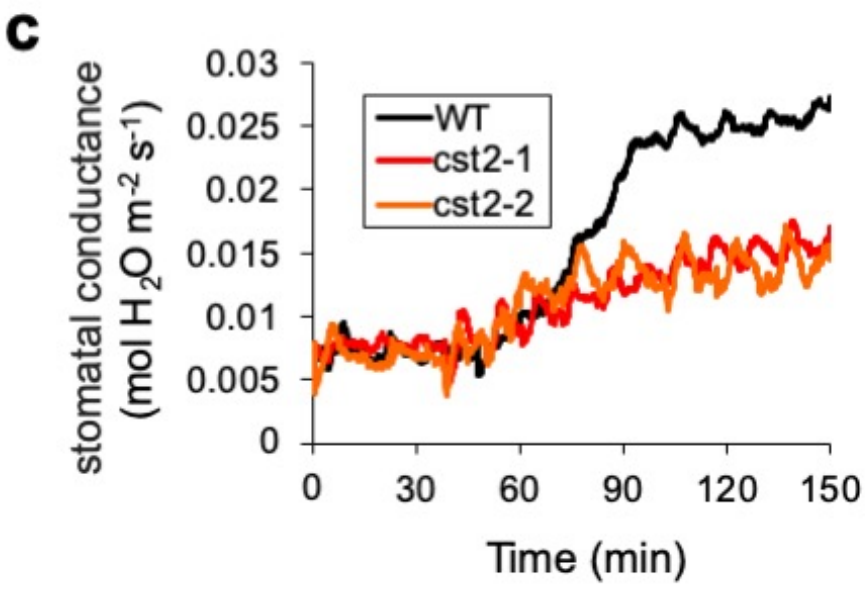


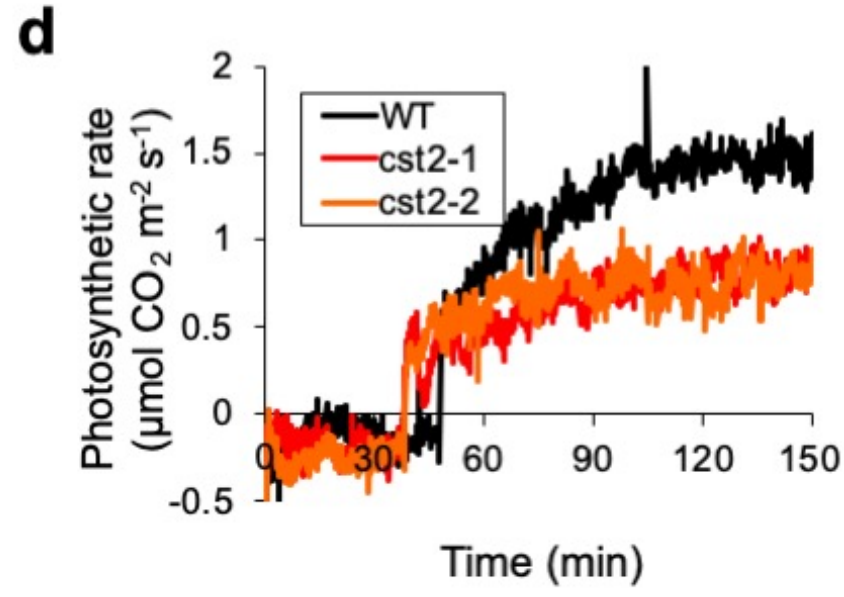


**Figure 5. Time-dependent change of stomatal opening in response to high Mg**

**a,** Light- and Mg-dependent stomatal opening in WT and *cst2* mutant. Plants were grown in hydroponic medium containing various Mg concentrations for 28-32 days. Epidermal fragments were isolated from dark-adapted plants and irradiated by the mixed light for 3 h as described in Figure 1b. Data represent the mean ± SD of 3-5 experiments. Each experiment used 30 stomata. Asterisks indicate statistically significant differences from the corresponding WT control using Two-way ANOVA by Tukey's multiple comparisons test (*P < 0.05, **P < 0.01, ***P < 0.001).

**b,** Time-course of stomatal opening capacities of WT and *cst2* mutants in response to high Mg treatment. Plants were grown hydroponically in 0.2 mM Mg conditions for 4 weeks, followed by transferring to 5 mM Mg. Rosette leaves were harvested 3 h after the start of the light period. Epidermal fragments were immediately isolated and stomatal apertures were determined by microscopy. Data represent the mean ± SD of 4 experiments. Each experiment used 30 stomata. Asterisks indicate statistically significant differences from corresponding WT control using Two-way ANOVA by Tukey's multiple comparisons test (*P < 0.05, ***P < 0.001).

**c and d,** Changes in stomatal conductance (**c**) and photosynthetic rate (**d**) in response to light in leaves of WT and *cst2* mutants. Plants were grown for 5 d in 5 mM Mg solution, followed by maintaining in the dark overnight prior to measurements at the fifth day morning. White light at 1000 μmol $m^{-2}$ $s^{-1}$ was applied to the upper surface of a leaf. Experiments repeated on two occasions gave similar results.

Figure 6

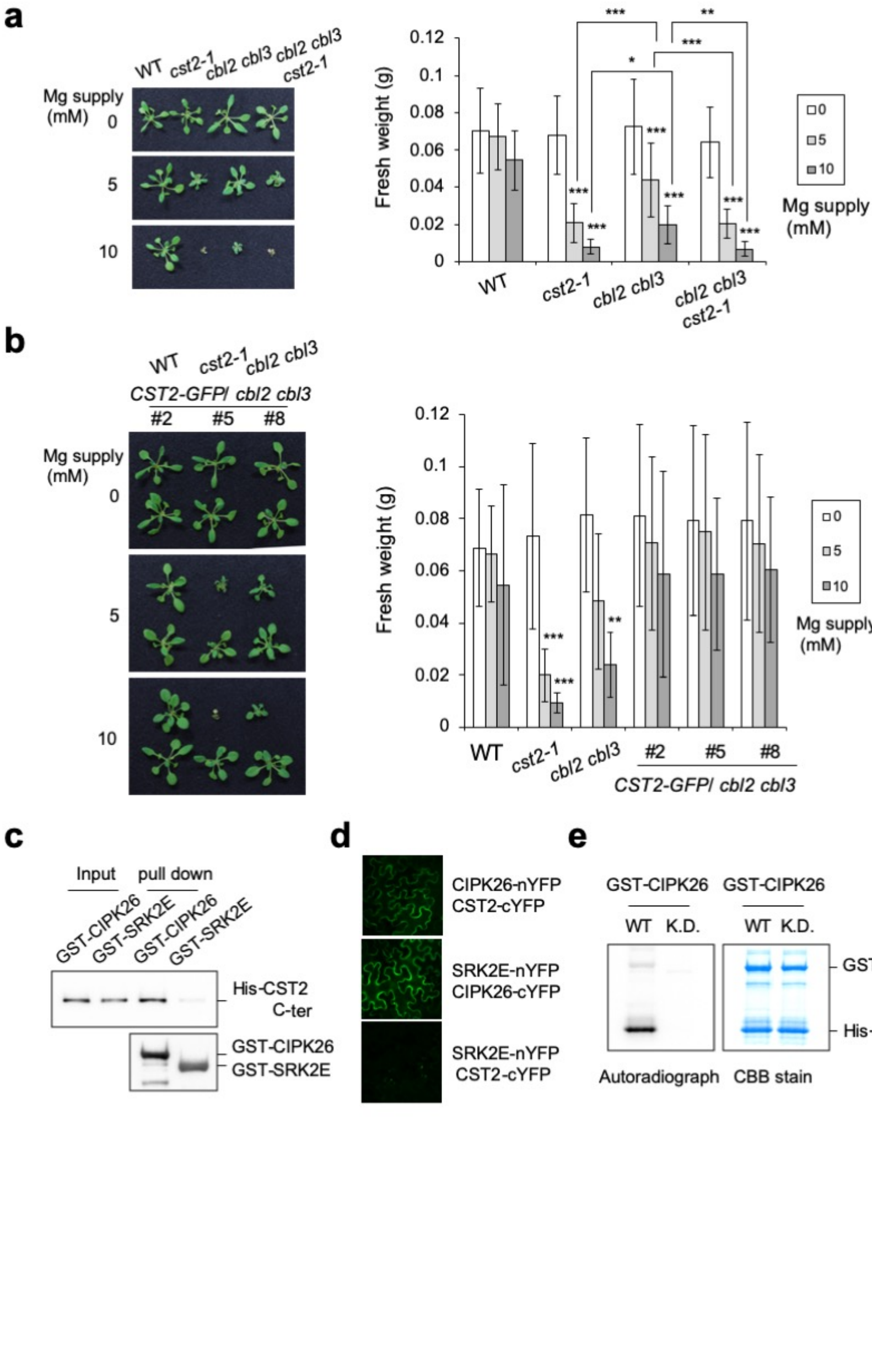
a
WT
cst2-1
cbl2 cbl3
cbl2 cbl3 cst2-1
Mg supply (mM)
0
5
10
Fresh weight (g)
0.12
0.1
0.08
0.06
0.04
0.02
0
***
**
*
WT
cst2-1
cbl2 cbl3
cbl2 cbl3 cst2-1
0
5
10
Mg supply (mM)
b
WT
cst2-1
cbl2 cbl3
CST2-GFP/ cbl2 cbl3
#2
#5
#8
Mg supply (mM)
0
5
10
Fresh weight (g)
0.12
0.1
0.08
0.06
0.04
0.02
0
***
**
WT
cst2-1
cbl2 cbl3
#2
#5
#8
CST2-GFP/ cbl2 cbl3
0
5
10
Mg supply (mM)
c
Input
pull down
GST-CIPK26
GST-SRK2E
GST-CIPK26
GST-SRK2E
His-CST2 C-ter
GST-CIPK26
GST-SRK2E
d
CIPK26-nYFP
CST2-cYFP
SRK2E-nYFP
CIPK26-cYFP
SRK2E-nYFP
CST2-cYFP
e
GST-CIPK26
GST-CIPK26
WT
K.D.
WT
K.D.
GST-CIPK26
His-CST2 Ct
Autoradiograph
CBB stain

**Figure 6. Genetic and physical interaction between CST2 and CBL-CIPK.**
**a**, Growth of WT, *cst2-1*, *cbl2 cbl3*, *cbl2 cbl3 cst2-1* (left), and shoot fresh weight (right) of the plants at different Mg concentrations. Asterisks indicate statistically significant differences using Two-way ANOVA by Tukey's multiple comparisons test (*P < 0.05, **P < 0.01, ***P < 0.001). Asterisks just on each error bar show significant differences comparison with corresponding WT control. **b,** Growth of WT, *cst2-1*, *cbl2 cbl3*, *CST2-GFP/cbl2 cbl3* lines (#2, #5, #8) (left), and shoot fresh weight (right) of the plants at different Mg concentrations. Plants were grown in 1/2 MS containing agar medium for 7 d and then transferred to a new 1/2 MS containing agar medium with or without Mg supply at indicated concentrations. Plants were further grown for 2 weeks. Data represent the mean ± SD (n = 22-32 for (**a**) and
n = 21-34 for (**b**)). Asterisks indicate statistically significant differences from WT control using Two-way ANOVA by Tukey's multiple comparisons test (**P < 0.01, ***P < 0.001).
**c**, *In vitro* pull-down assay for the interaction of CST2 with CIPK26. Recombinant GST-CIPK26, GST-SRK2E, and His-CST2 C-terminal region (CST2 C-ter) were expressed in *E. coli*. Extract from the *E. coli* cells expressing GST-CIPK26 or GST-SRK2E was mixed with that expressing His-CST2 C-ter and reacted with glutathione-Sepharose 4B beads. The proteins on the beads were subjected to SDS-PAGE and then immunoblotted using anti-GST and anti-His antibodies.
**d**, *In vivo* interaction of CST2 with CIPK26 determined by a bimolecular fluorescence complementation (BiFC) assay. CIPK26, SRK2E, CST2 constructs were co-transformed with indicated combinations into *Nicotiana benthamiana* leaves. The reconstituted fluorescent signal was observed using a confocal laser microscope. Co-expression of SRK2E with CIPK26 is a positive control. nYFP and cYFP represent the N- and C-terminal halves of the YFP protein, respectively.
**e**, *In vitro* phosphorylation of CST2 by CIPK26. Autoradiograph (left) and CBB stain (right) of gel were shown. CST2 C-ter was reacted with WT GST-CIPK26 or kinase dead (K.D.) GST-CIPK26 in the presence of $P^{32}$ATP to detect the CIPK26-mediated phosphorylation.

Figure 7

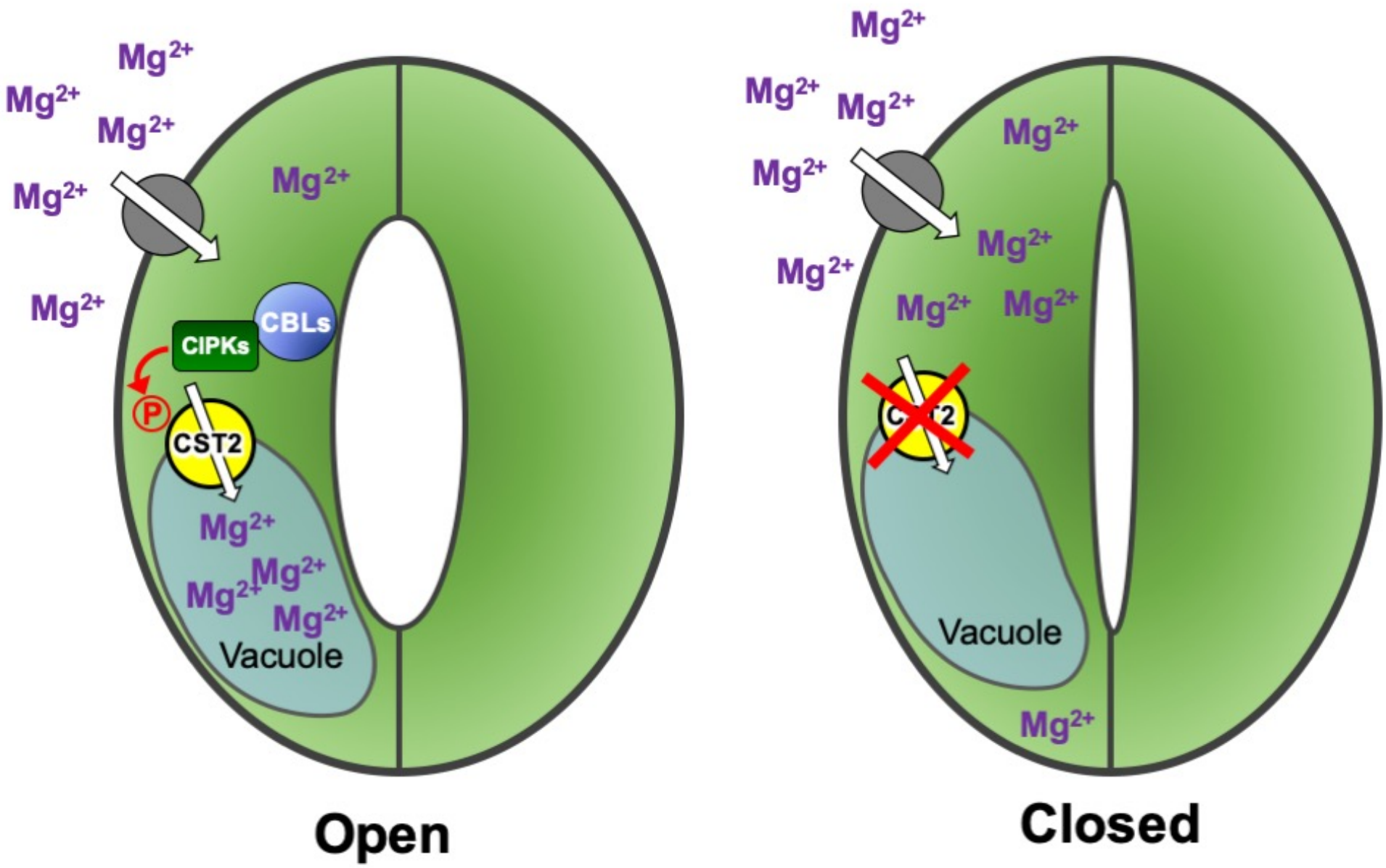


**Figure 7. Schematic presentation of CST2 role in stomatal opening**
Mg concentration in cytosol of stomatal guard cells is maintained at a steady level by different ways. One of them is to sequester Mg into vacuole by CST2 localized at the tonoplast to maintain Mg homeostasis, which is important for stomatal opening (left). Knockout of CST2 results in stomatal closure due to high Mg in the cytosol in the guard cells (right). CST2 is phosphorylated by CBL-CIPK26.

# Supplementary Figure 1

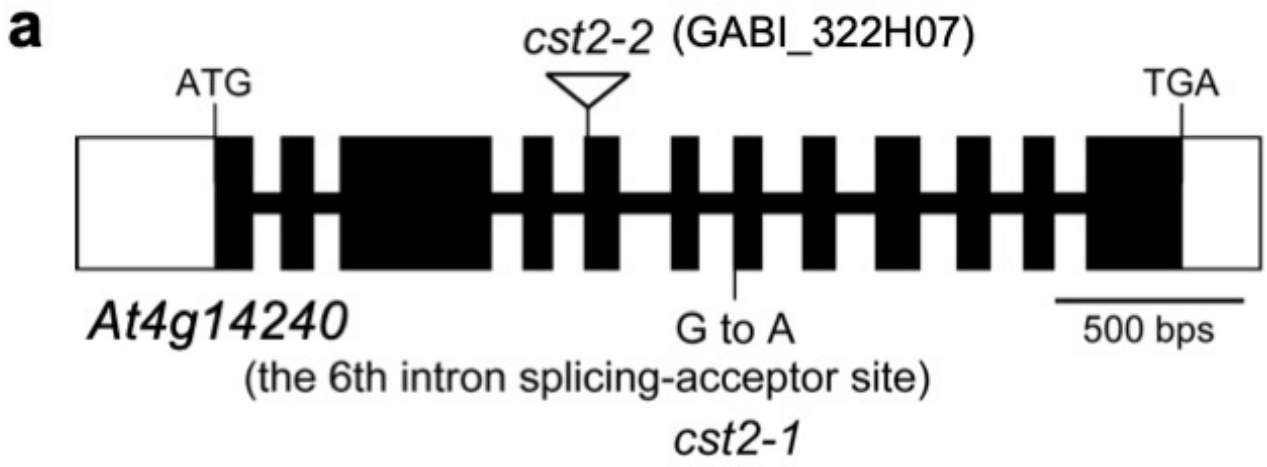


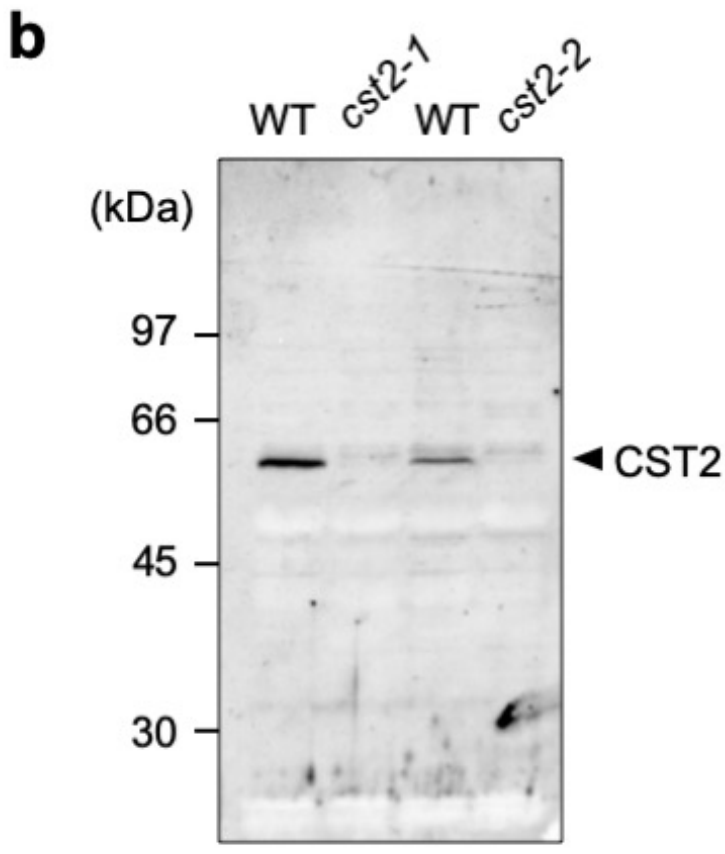



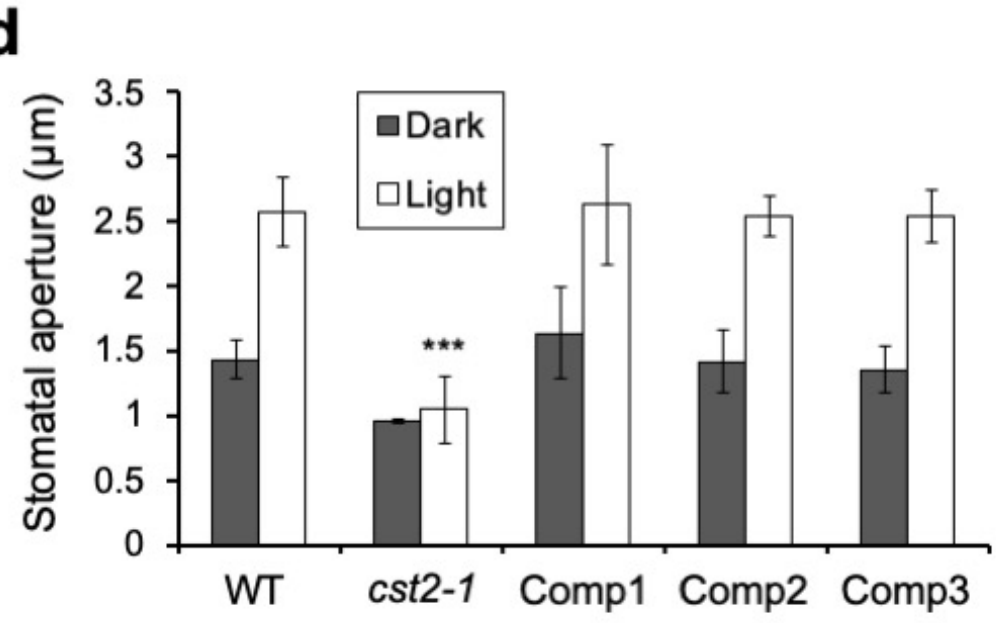


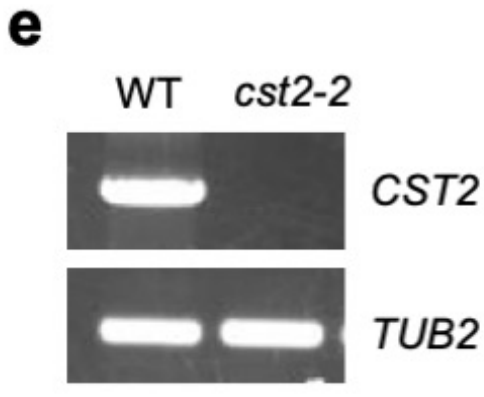


**Supplementary Figure 1. Gene mapping, structure and complementation test**
a, Genomic structure of the *CST2* gene. Position of the *cst2-1* mutation and the site of T-DNA insertion in *cst2-2* (GABI_322H07) are indicated. Boxes and lines represent exons and introns, respectively. T-DNA was inserted in the fifth exon for *cst2-2*.
**b,** Expressions of CST2 protein in rosette leaves of WT and *cst2* mutants. Immunoblotting was performed.
**c and d,** Complementation of growth defect (**c**) and impairment stomatal opening (**d**) in the *cst2-1* mutant with a wild-type genomic *CST2* gene. WT, *cst2-1* and *cst2-1* plants harboring a transgene with the WT *CST2* gene (Comp1 to 3) were grown on soil for 4 weeks. Light-dependent stomatal opening was measured as described in Figure 1b. Data represent the mean ± SD of triplicate experiments. Each experiment used 30 stomata. Asterisks indicate statistically significant differences from WT control using Two-way ANOVA by Tukey's multiple comparisons test (***P < 0.001).
**e,** Expression of *CST2* in rosette leaves of WT and *cst2-2* plants. RT–PCR analysis was performed. *TUB2* was used as an internal control.

# Supplementary Figure 2

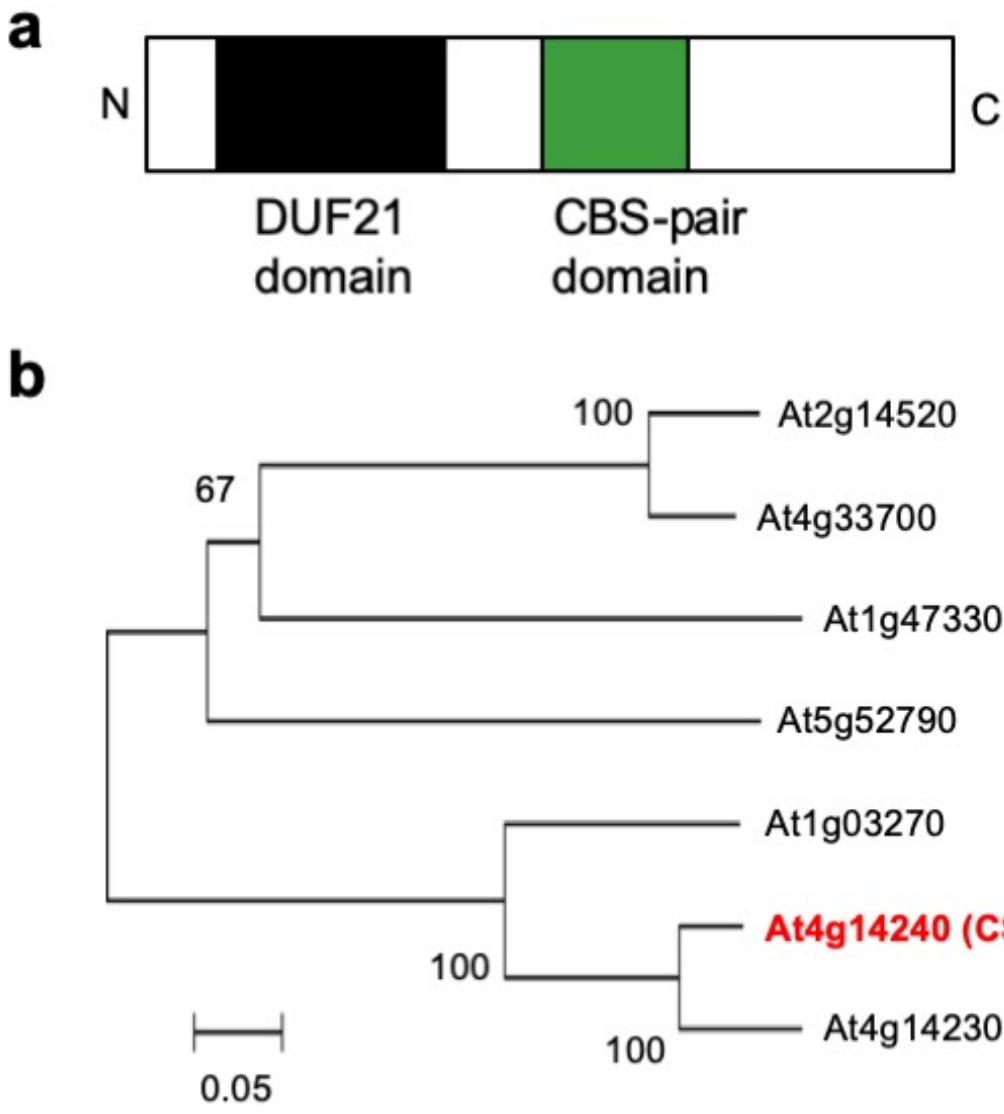


**Supplementary Figure 2. Structure and phylogenetic tree of CST2.**
**a,** Schematic representation of the CST2 protein. CST2 protein has a DUF21 and CBS-pair domains.
**b and c,** Phylogenetic relationships between CST2 and homologous proteins from Arabidopsis thaliana (**b**) and from other organisms (**c**). The alignment was performed using the MUSCLE (Edgar, 2004) with full length amino acid sequences. The tree was constructed using MEGAX software with the neighbor-joining method. The Arabidopsis CST2 is shown in bold red letters. Yeast MAM3 is shown in bold letters. The numbers next to the branches are bootstrap values (1,000 replicates). The scale bar represents 0.05 (**b**) or 0.2 (**c**) substitutions per site.

Supplementary Figure 3

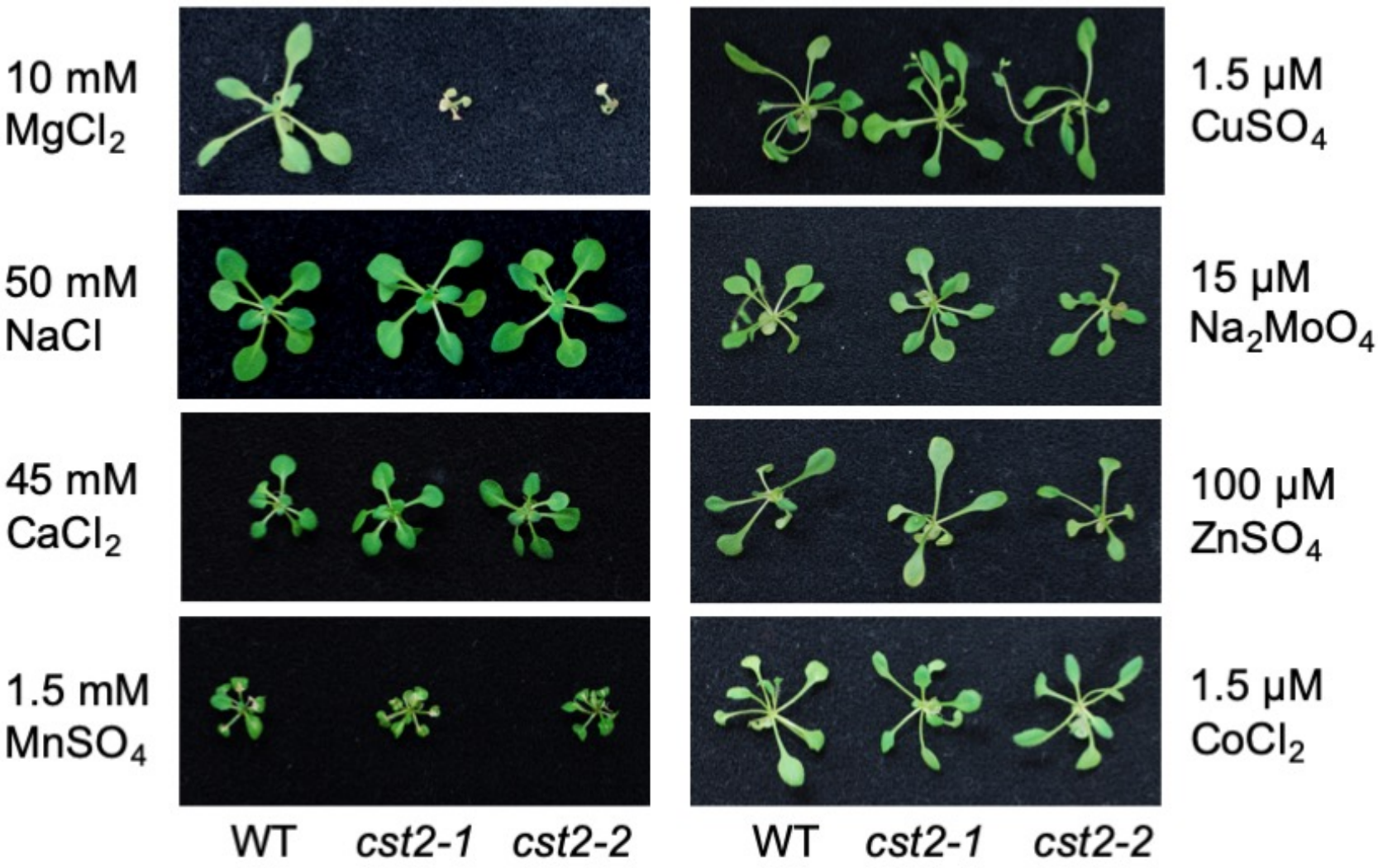


**Supplementary Figure 3. Growth of wild type (WT) and *cst2* mutants grown under different ionic stress conditions**

Plants were grown in 1/2 MS containing agar medium for 7 days and then transferred to a new 1/2 MS containing agar medium containing different ions as indicated for a further 2-weeks.

Supplementary Figure 4

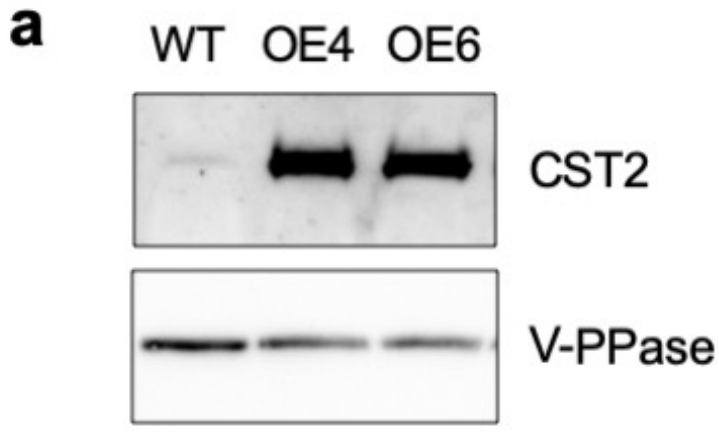


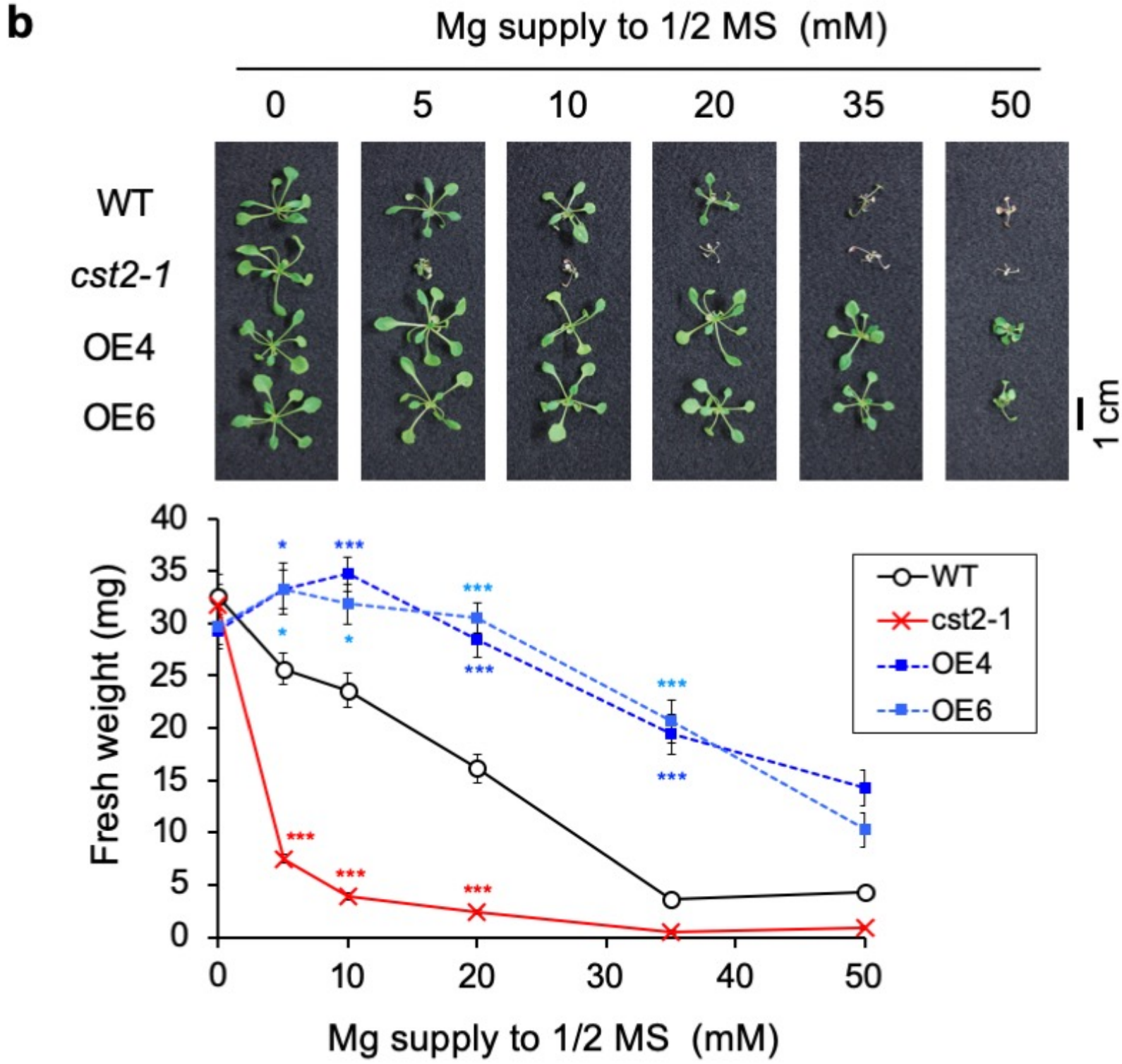


**Supplementary Figure 4. Growth response of CST2-overexpressing plants to high Mg**
**a,** Expressions level of CST2 protein in rosette leaves of WT and the overexpression lines (OE4 and OE6). Immunoblotting was performed.
**b,** Mg concentration-dependent growth of WT, *cst2-1* mutant, and CST2 overexpressing lines (OE4 and OE6). Plants were grown on 1/2 MS containing agar medium containing different Mg concentrations. After 22 days growth, the plants were photographed and the shoot fresh weight was recorded. Data represent the mean ± SD (n = 10-25). Asterisks indicate statistically significant differences from WT control using Two-way ANOVA by Tukey's multiple comparisons test (*P < 0.05, ***P < 0.001).